Gas Turbine Laboratory
Department of Aeronautics and Astronautics
Massachusetts Institute of Technology
Cambridge, MA 02139

A Final Progress Report on Grant NAG3-2767

entitled

TURBOMACHINERY FOR LOW-TO-HIGH MACH NUMBER FLIGHT

submitted to

NASA Glenn Research Center
21000 Brookpark Rd.
Cleveland, OH 44135

ATTN: Dr. Kenneth Suder

PRINCIPAL INVESTIGATOR: Dr. Choon S. Tan
Senior Research Engineer, Gas Turbine Laboratory

Research Assistant: Parthiv N. Shah

PERIOD OF INVESTIGATION: April 1, 2002 to March 31, 2004.

This page is intentionally left empty

Table of Content

This page is intentionally left empty

TURBOMACHINERY FOR LOW-TO-HIGH MACH NUMBER FLIGHT

Executive Summary

The thrust capability of turbojet cycles is reduced at high flight Mach number (3+) by the increase in inlet stagnation temperature. The 'hot section' temperature limit imposed by materials technology sets the maximum heat addition and, hence, sets the maximum flight Mach number of the operating envelope. Compressor *pre-cooling*, either via a heat exchanger or mass-injection, has been suggested as a means to reduce compressor inlet temperature and increase mass flow capability, thereby increasing thrust. To date, however, no research has looked at ***compressor cooling*** (i.e., using a compressor both to perform work on the gas path air and extract heat from it simultaneously). We wish to assess the feasibility of this novel concept for use in low-to-high Mach number flight.

The results to-date show that an axial compressor with cooling: (1) relieves choking in rear stages (hence opening up operability), (2) yields higher-pressure ratio and (3) yields higher efficiency for a given corrected speed and mass flow. The performance benefit is driven: (i) at the blade passage level, by a decrease in the total pressure reduction coefficient and an increase in the flow turning; and (ii) by the reduction in temperature that results in less work required for a given pressure ratio. The latter is a thermodynamic effect. The impact of the location of cooling within the compressor (i.e. front or back) has also been examined.

As an example, calculations were performed for an eight-stage compressor with an adiabatic design pressure ratio of 5. By defining non-dimensional cooling as the percentage of compressor inlet stagnation enthalpy removed by a heat sink, the model shows that a non-dimensional cooling of 1percent in each blade row of the first two stages can increase the compressor pressure ratio by as much as 10-20 percent. Maximum corrected mass flow at a given corrected speed may increase by as much as 5 percent. In addition, efficiency may increase by as much as 5 points.

A framework for characterizing and generating the performance map for a cooled compressor has been developed. The approach is based upon CFD computations and meanline analysis. Figures of merit that characterize the bulk performance of blade passage flows with and without cooling are extracted from CFD solutions. Such performance characterization is then applied to a preliminary compressor design framework (meanline). The generic nature of this approach makes it suitable for assessing the effect of different types of compressor cooling schemes, such as heat exchange or evaporative cooling (mass injection).

Future work will focus on answering system level questions regarding the feasibility of compressor cooling. Specifically, we wish to determine the *operational/parametric space* in which compressor cooling would be advantageous over other high flight Mach number propulsion concepts. In addition, we will explore the *design requirements* of cooled compressor turbomachinery, as well as the *flow phenomena* that limit and control its operation, and the *technology barriers* that must be crossed for its implementation.

1.0 Background, Motivation and Scope

The large majority of research on turbomachinery has focused aircraft turbine engine applications. The resulting scientific basis has enabled the design and development of turbo machinery components with improved performance at lower cost and in reduced time for aircraft gas turbine engine applications. Turbomachinery for wide flight Mach number applications such as that needed to access space, however, must operate under very different conditions of temperature, pressure and mass flow. Specifically this type of turbomachinery must meet performance requirements along an ever changing set of flight Mach numbers, and hence, inlet stagnation temperatures and pressures; this is in direct contrast to the fixed design point 'cruise' type missions that most aircraft engine turbomachinery components are optimized for. A key requirement of the earth-to-space propulsion system is providing high thrust at acceleration, which at high-Mach number flight is set by the airflow. Thus the use of turbofan/turbojet over a wide Mach number range would be required to meet two key criteria: (1) matching of the inlet flow delivery capability to the maximum engine flow capability, and (2) matching the engine thrust profile to that of the flight-vehicle drag. Because of the large inlet area needed to provide the necessary high Mach number airflow, mismatch of the fan and compressor to inlet can be expected at low flight Mach number.

An increase in flight Mach number implies rising recovered temperature, thus leading to lowering in corrected mass flow, falling corrected speed (and this effect could be exacerbated by the need to reduce rotation-induced stress due to the associated rising compressor delivery temperature) and hence lowering in the compressor pressure ratio. The net effect is thus a loss of thrust in a flight regime where the flight vehicle drag could still be high; this could bring upon an overall penalty in fuel burn as well as the low usage of available airflow. Thus the compressor needs both a robust inlet airflow delivery system and a performance capability at a wide range of mechanical speeds.

Another constraint imposed on the use of turbomachinery-based airbreathing propulsion system for high Mach number flight is the limitation on heat addition into the air stream that has already been "heated" due to ram compression. For example the performance of a turbojet with fixed turbine inlet temperature would deteriorate as the flight Mach number increases, thus imposing a limit on the speed range achievable. This limit on flight Mach number range, which can somewhat be extended with afterburning, is primarily due to: (1) poor performance of compressor that affects the expansion ratio in the nozzle on account of the heated stream from ram compression; and (2) reduction in the amount of heat that could be added (this can be mitigated in an Air TurboRocket Cycle where high-pressure propellants – either burnt in a rocket-like combustion chamber or vaporized and heated by heat exchange with combustion products – expand through turbine that drives the compressor). However if the heat from the air delivered to the compressor is extracted by the use of a suitably-designed heat exchanger, the performance of the compressor could improve (significantly) and the limit on the amount of heat that can be added to the air stream can be alleviated. Removing heat from ram-compressed air stream reduces the power required for a given compression ratio, the throughflow area required for a given mass flow rate, and the severity of the environment imposed on the compressor. This allows an increase in the maximum allowable flight Mach number beyond what would otherwise be possible within the same material, structural and thermal limits inherent in turbomachinery-based airbreathing propulsion system. There are two ways of heat extraction from the air stream: one is on the use of a separate heat exchanger located upstream of the compressor (i.e. precooling the compressor) to reduce the temperature of the air into the compressor, and the other is on using the compressor itself as a heat exchanger (i.e. compressor cooling) to extract heat as the air flow though the compressor flow paths.

Precooling the compressor requires the use of a heat exchanger that has the following constraints: the associated pressure drop/loss, its additional weight, its installation (requiring additional real estate on the engine) with the size limited by inlet capture area or propulsion system envelop. These constraints further confine the trade between heat transfer and pressure

loss. By contrast use of compressor cooling would remove some of the constraints imposed upon by the use of compressor precooling. The engineering challenge here would then be developing the technology for compressor blade cooling and sources of heat sink. Hybrid system consisting of precooling followed by compressor cooling could also be considered.

The pressure ratio requirement on the compressor also changes with flight speed. At high flight speed the compression from ram effect reduces the compressor pressure ratio requirement whereas at low flight speed, compressor must provide the required pressure ratio. Means would have to be developed to cope with this changing pressure ratio requirement. Another alternative would be the engineering of compressor blades such that boundary layer can be removed (i.e. aspiration) at low flight speed (thus enabling highly loaded compressor stage to produce the high pressure ratio needed) while at high speed the aspiration can be turned off (and perhaps coolant introduced to protect the blade) as the compressor stage loading requirement diminishes [Strazisar and Adamczyk of NASA GRC, 2003]. Active stabilization of inlet-fan-compressor system should also be considered for mitigating and overcoming the operability limits.

There is thus a need to delineate the enabling design characteristics/attributes of turbomachinery for operation across wide flight Mach number ranges. The large change in inlet temperature and the resulting ram compression as the flight Mach number increases poses several key challenges that must be addressed adequately if the turbomachinery components are to maintain acceptable level of performance over the anticipated range of operation. The drivers that set the performance and operability of fan/compressor for wide flight Mach number range could be different from those of fans/compressors for subsonic and transonic flow regimes.

The technical challenges include management of losses (efficiency), cooling technology (i.e. thermal management) to deal with the large change in stagnation temperature encountered in high-speed flight, and inlet-fan-compressor operability when inlet delivers a non-uniform (perhaps even unsteady) flow involving temperature and pressure. To put the problem in NASA context, we can state the research areas of interest. The first concerns inlet-fan-compressor range and (aerodynamic as well as aeromechanic) stability, and the matching requirements over the flight range. Here there is a need to define the elements needed to develop the methodology for assessing the operability and performance of inlet-fan-compressor as a system on a first principle basis. The second is compressor performance in terms of maintaining acceptably high efficiency with adequate operability margins for providing the required pressure ratio over the range of flight speed to meet the mission thrust profile requirements; this is somewhat related to the first. The third is developing means of alleviating and overcoming the limitations imposed on the component performance and operability.

The present report describes the research that began in June 2002 on compressor cooling as an enabling aspect for turbomachinery for low-to-high Mach number flight. For completeness a brief review of selected work on turbomachinery-based high-speed propulsion systems. This is then followed by presenting results from

2.0 A Review of Selected Work on Turbomachinery-based High-speed Propulsion Systems

Variable cycle turbomachinery-based propulsion systems from takeoff to high-speed flight are reviewed and described in Heiser and Pratt[1994] and Johnson[1996]. Many concepts that are described fall under the heading of combined cycle engines, i.e., engines that integrate multiple propulsion concepts within the same internal flowpath. Different combined cycle concepts include the combination of turbofan/turbojets and ramjets (turboramjet), or the former plus a rocket motor (turbo ramjet rocket). A concept that is commonly found in the literature is the liquid air cycle engine (LACE), which uses cryogenic liquid hydrogen fuel to produce liquid air (oxidizer) via a heat exchanger, and then reacts the fuel and oxidizer inside a rocket engine to produce thrust. Another concept, the inverse cycle engine (ICE) also appears in various studies. This concept is unique in that the inlet airflow is first expanded through a turbine and then passed through a heat exchanger (cooler) before being compressed, burned and expanded through a nozzle. Both the turbine expansion and heat exchange processes serve to lower the compressor inlet temperature. Although capable of producing thrust at high Mach numbers, the ICE's main drawback is that it cannot produce adequate subsonic thrust, thereby preventing it from being a stand-alone system.

One concept that has potential as a stand-alone low-to-high Mach number propulsion system is the pre-cooled turbojet alluded to in Section 1.0, or the pre-cooled turbojet with reheat (afterburning). The use of pre-cooling to stretch the Single-Spool Turbojet(SSTJ) operating envelope to Mach 5 or 6 is not new, and is discussed in several sources (Hewitt and Johnson[1991], Powell and Glickstein[1988], Rudakov and Balepin[1991], Sreenath[1961]). As it potentially involves straightforward modifications to existing turbojet engines, it is an attractive concept in its own right.

The sources referred to in this literature review by no means form an exhaustive survey of wide Mach operation turbomachinery applications, but do represent a good cross-sectional sample of work to date on this topic.

3.0 Propulsion System Mission Requirements and Definition of a Sample Vehicle Trajectory

The first step in our system level analysis is to define a sample vehicle mission profile. At this stage, a mission profile corresponds to a trajectory definition in the altitude-Mach number plane. The trajectory for a low-to-high Mach number aircraft depends on the vehicle's intended mission. Several types of mission profiles could be considered for a wide flight Mach number vehicle: (1) a minimum fuel to climb mission may be appropriate for a two-stage-to-orbit (TSTO) vehicle, since minimizing fuel would permit the second stage to maximize payload; (2) a minimum time to climb mission may be appropriate for an advanced fighter/interceptor aircraft; (3) a constant dynamic pressure mission may be appropriate for vehicle structural reasons. These different mission profiles imply different propulsion system operating conditions. At the component level, it will be necessary to characterize the implications on the turbomachinery (e.g., compressor) performance. This will be addressed for both (1) adaptation of technology for wide flight Mach number ranges on an existing SSTJ and (2) design and development of an entirely new turbomachinery-based propulsion system.

To begin, we establish a baseline mission profile by examining a flight vehicle climbing along a nearly constant dynamic pressure ($q = \rho V^2/2$) trajectory of 0.28 atmospheres, from Mach number zero to ``high" Mach numbers of 4 or 5. The other two criteria, namely, minimum fuel to climb and minimum time to climb will be addressed in future work. Figure 1 shows the trajectory in the altitude-Mach number plane. At ``lower" Mach numbers the trajectory is defined by the broken line, while at ``high" Mach numbers the trajectory follows a line of constant q. The dynamic pressure selected for the high Mach number portion of the trajectory corresponds to

M=4 at an altitude of 25 km, and falls within design ranges typically given in the literature [Johnson (1995)].

A standard atmosphere model has been used to define the ambient air properties along the flight path [Anderson (1989)]. Figure 2 shows the temperature, pressure, and density as functions of altitude, as well as contours of constant Mach number in the altitude-velocity plane. The change in total temperature (T_t) and total pressure (p_t) along the flight path is shown in figures 3 and 4, respectively. The rapid increase in T_t with Mach number is the primary reason that standard single-spool turbojet (SSTJ) technology fails to produce thrust at high Mach numbers. Current material temperature limits in both the compressor, and especially the turbine limit the production of thrust by reducing the heat addition capability of the fuel in the combustor. Cooling the air to regain this heat addition capability would therefore be a logical cycle enhancement for wide Mach number applications. The next section gives one example of this type of cycle enhancement using a pre-cooler.

4.0 Ideal Cycle Mission Analysis of SSTJ with Pre-cooling

4.1 Modification of Ideal SSTJ Cycle for Compressor Pre-cooling

A schematic of the ideal pre-cooled SSTJ is shown in Figure 5. Station 0 represents the engine inlet. Because stagnation properties are assumed not to change within an *ideal* inlet, station 0 is also the pre-cooler entrance. Station 2 is the pre-cooler exit/compressor inlet. Station 3 is the compressor exit/combustor inlet. Station 4 is the combustor exit/turbine inlet; Station 5 is the turbine exit. Station 7 is the nozzle exit.

An expression for the specific thrust of the ideal SSTJ cycle with pre-cooling can be obtained by performing an ideal design point cycle analysis. This can be written in terms of the controlling non-dimensional parameters M_0, θ_t, θ_0, τ_c and τ_x as shown in equation (1):

$$\left(\frac{T}{\dot{m}a_0}\right)_{available} = \sqrt{\frac{2\theta_0}{\gamma-1}\left(\frac{\theta_t}{\theta_0\tau_c}-\tau_x\right)+\frac{\theta_t M_0^{\,2}}{\theta_0\tau_c}} - M_0 \qquad (1)$$

where the specific thrust, $\left(\frac{T}{\dot{m}a_0}\right)$, consists of:

- T, the thrust.
- $\dot{m}$, the airflow through the engine.
- a_0, the local speed of sound.

The right hand side of equation (1) consists of
- M_0, the vehicle's flight Mach number
- $\theta_t = T_{t4}/T_0$, the turbine inlet temperature, T_{t4}, normalized by the ambient temperature, T_0.
- $\theta_0 = T_{t0}/T_0 = 1+\{(\gamma-1)/2\}M_0^2$, the ram temperature rise coefficient.
- $\tau_c = T_{t3}/T_{t2}$, the compressor temperature ratio.
- $\tau_x = T_{t2}/T_{t0}$, the pre-cooler temperature ratio.

Equation 1 has been derived assuming:

1. Airflow through the engine can be modeled as a perfect gas (c_p = constant, γ=1.4)

2. All standard SSTJ components are lossless: inlet, compressor, combustor, turbine, nozzle (Note that under the lossless compressor assumption, cycle compressor pressure ratio is related to the cycle temperature ratio by the isentropic relation $\tau_c = \pi_c^{[(\gamma-1)/\gamma]}$).
3. An ideal pre-cooler consisting of a lossless, constant-pressure heat exchanger is located upstream of the compressor.
4. Fuel flow is small compared to mass flow $\left(\dot{m}_{fuel} << \dot{m}_{air} \approx \dot{m}\right)$.
5. Flow through the nozzle is isentropically expanded to ambient pressure.

Typically, a cycle is defined by the turbine inlet temperature, T_{t4}, the compressor pressure ratio, π_c, and the vehicle trajectory. Along with the trajectory defined in section 3.0, the following values of T_{t4} and π_c were chosen to represent aggressive, but achievable technology levels:

$T_{t4} = 2300K$
$\pi_c=8$

The pre-cooler exit to inlet temperature ratio, $\tau_x = T_{t2}/T_{t0}$, characterizes the heat transfer. By setting $\tau_x=1$ (i.e., no pre-cooling), we recover the equation for the standard ideal SSTJ cycle specific thrust [Kerrebrock(1992)]. For cooling, this ratio is less than unity. It is clear, then, that the lower this ratio is, the greater the increase in specific thrust.

As an example figure 6 shows the specific thrust of an uncooled $\tau_x=1$ vs. pre-cooled $\tau_x=0.8$ SSTJ having the given T_{t4}, π_c, and the trajectory described in section 3. From the figure, we see that specific thrust falls off as flight Mach number increases. Eventually, the specific thrust falls off to zero as the critical Mach number is reached. This is directly attributable to the increase in compressor inlet stagnation temperature, T_{t2}, which correspondingly results in increased compressor exit temperature, T_{t3}. Since the turbine inlet temperature, T_{t4}, is fixed by material temperature limits, the effect of higher flight Mach number is to reduce the potential to add energy (T_{t4} - T_{t3}) in the combustor, and hence, to reduce the specific thrust. It is clear from the figure that pre-cooling both increases the specific thrust and also increases the maximum Mach number at which thrust can be generated. It should be noted that the specific thrust in figure 6 is shown for a non-dimensional, ``rubber'' engine, whose inlet and nozzle geometry would have to be capable of changing area along the flight path in order to remain ``on-design''. The next section revisits this point.

The heat transfer is related to the temperature drop across the pre-cooler normalized by the pre-cooler inlet stagnation temperature, $\Delta T/T_{t0}$. The heat transfer rate can be conveniently defined in terms of cycle variables as:

$$\frac{\Delta T}{T_{t0}} = \frac{\dot{q}}{c_p T_{t0}} = \frac{\dot{Q}}{\dot{m} c_p T_{t0}} = \tau_x - 1 \qquad (2)$$

Besides the specific thrust, the *specific impulse*, $I_{sp} = T/\left(\dot{m}_{fuel} g\right)$, i.e., the cycle's ability to convert fuel into thrust, is also of interest. Other studies on pre-cooling have generally focused on balancing the cooling requirement with the fuel available as coolant [Hewitt et al.(1991), Powell et al.(1988), Rudakov et al.(1991), Sreenath(1961)]. In the SSTJ with afterburning, pre-cooling is often achieved by overfueling (fuel equivalence ratio, $\phi>1$), with the excess fuel dumped into the afterburner. Sreenath(1961) has also considered carrying water on board for cooling and then eventually recovering a small amount of thrust from it. Depending upon the equivalence ratio and the fuel/coolant selection, the specific impulse of pre-cooled turbojets ranges from hundreds to thousands of seconds in the literature. As we have not yet chosen to

consider the engineering of a heat exchanger to achieve the required pre-cooling, a discussion of specific impulse is not included in this report. This point will be addressed in future work.

4.2 Example: Achieving Mission Required Specific Thrust Using Pre-cooling

The propulsion system must generate thrust levels that enable the vehicle to climb from Mach zero at sea level to Mach 4 or 5 at an altitude of 25km. Here, as a simplification we first consider the minimum required specific thrust. The minimum required thrust has been estimated by considering a vehicle in steady, level flight everywhere along the selected trajectory shown in figure 1. Under these conditions, the vehicle weight must equal the lift and the thrust must equal the drag:

$$W = L = C_L q_\infty S \tag{3}$$

$$T = D = C_D q_\infty S \tag{4}$$

so that

$$C_L = \frac{W/S}{q_\infty} \tag{5}$$

In equation 3 to 5, q_∞ is the dynamic pressure and is given by:

$$q_\infty = \frac{\rho_0 V_0^2}{2} = \frac{\gamma p_0 M_0^2}{2} \tag{6}$$

The vehicle drag consists of the zero-lift drag coefficient, C_{D0}, and the drag due to lift (induced drag):

$$C_D = C_{D_0} + K\left(\frac{W/S}{q_\infty}\right)^\eta \tag{7}$$

Along the flight path, the coefficients, C_{D0}, K and η in equation 7 are functions of the flight Mach number only. However, the definition of vehicle reference area, S, which is ultimately the engineer's choice, affects the actual value of the coefficients. For two vehicles having a consistent vehicle reference area definition, the vehicle drag model is completely scalable. When choosing these coefficients for preliminary analysis, then, the class of vehicle is important (e.g., a high performance aircraft versus a hypervelocity glider). The drag model chosen in this analysis was based upon the aerodynamic characteristics of a typical jet aircraft at supersonic speeds [Miele (1962)], and is shown in figure 7.

Assuming that flow into the compressor is purely in the axial direction and nowhere choked, the ideal mass flow can be determined by the vehicle trajectory variables (p_0, T_0, and M_0), the pre-cooling temperature ratio (τ_x), the compressor face Mach number (M_C), and the compressor face area (A_C). The expression for the mass flow is given by equation 8.

$$\dot{m} = \sqrt{\frac{\gamma}{R}}\frac{A_c p_0}{\sqrt{T_0}}\frac{1}{\sqrt{\tau_x}} M_c \left[\frac{1+\frac{\gamma-1}{2}M_0^2}{\frac{\gamma+1}{2}M_c^2}\right]^{(\gamma+1)/2(\gamma-1)} \tag{8}$$

What is interesting to note is that the ideal mass flow varies inversely with the square root of the pre-cooling ratio. Hence, more pre-cooling at constant-pressure allows greater mass flow to be ingested by the engine if the other variables are held fixed. For the vehicle in this example, the trajectory variables are given by the mission profile. The compressor face area and compressor face Mach number are assumed to be constant and have the values:

$$A_c = 1 \text{ m}^2$$
$$M_c = 0.6$$

It should be noted that the compressor face area, A_c, is the only engine geometric variable present in this analysis. Other than A_c, all other engine components are assumed to be ``rubber", implying that they are capable of changing geometry as necessary to satisfy the lossless component assumption and keep the engine ``on-design" at all points along the mission. It should also be noted that the assumption of fixed compressor face area and Mach number fix the orrected flow on the compressor map. By also having selected the cycle pressure ratio, π, to be fixed at a value of 8, we have effectively fixed the compressor operating point throughout the mission. With these assumptions, finally, the following expression can be derived for the required specific thrust, assuming an ideal, ``rubber" engine everywhere except at the compressor inlet:

$$\left(\frac{T}{\dot{m}a_0}\right)_{required} = \frac{\left[C_{D_0} + K\left(\frac{W/S}{q_\infty}\right)^n\right]}{2}\left(\frac{S}{A_c}\right)\left(\frac{M_0^2}{M_c}\right)\sqrt{\tau_x}\left(\frac{1+\frac{\gamma-1}{2}M_c^2}{\frac{\gamma}{2}M_0^2}\right)^{(\gamma+1)/2(\gamma-1)} \qquad (9)$$

This expression shows that in addition to increasing the cycle available specific thrust, as shown in the previous section, the presence of an ideal pre-cooler reduces the required specific thrust by the square root of the pre-cooling temperature ratio, $\sqrt{\tau_x}$. This can be directly attributable to the greater mass flow capability from cooling shown in equation 8.

The mission requirements are met when:

$$\left(\frac{T}{\dot{m}a_0}\right)_{available} \geq \left(\frac{T}{\dot{m}a_0}\right)_{required} \qquad (10)$$

Figures 8-11 show an example of a vehicle having W=980,000 N and S=276 m^2, on the given trajectory. The chosen wing loading, (W/S) is similar to an SR-71 (W ~ 624,000 N, S~ 170 m^2) or an F-16 fighter aircraft [Anderson(1989)] in steady, level flight at full takeoff weight. It is assumed, for simplicity, that the vehicle mass is constant on all points along the trajectory[1]. The dynamic pressure-to-wing loading ratio, a quantity which appears in equation 7 and 9, is:

$$\left(\frac{q_\infty}{W/S}\right) \approx 8$$

Figure 8 shows that without cooling, the required cycle specific thrust (dashed line) is greater than the available cycle specific thrust (solid line), and that this difference can be eliminated by the correct amount of pre-cooling (dash-dot line). The dash-dot curve is the locus of points that matches required specific thrust and the cycle available thrust through sufficient pre-cooling. From this figure, it is clear that pre-cooling can both augment specific thrust to satisfy mission requirements, and also expand the Mach number range (operating envelope) of a given engine cycle.

Figure 9 shows the value of the pre-cooler temperature ratio required to make the available and required specific thrusts match. Figure 10 shows the required pre-cooling in terms of temperature change, ΔT, and figure 11 shows it in terms of energy transfer rate. It can be seen that the required temperature change is on the order of ~100 K, and the required heat transfer is on the order of tens of megawatts.

---

[1] Fuel consumption causes the vehicle weight to decrease as the chosen mission progresses, thereby reducing the required specific thrust at higher Mach numbers. Accounting for fuel consumption would theoretically increase the vehicle's Mach envelope. As this example is designed by the author primarily to demonstrate the effect of an ideal pre-cooler, the effect is neglected at present.

4.3 Implications on Potential Cycle Benefit from Pre-cooling

From the ideal analysis it appears that the following conclusions can be drawn regarding the potential cycle benefit from pre-cooling:

1. Pre-cooling can potentially increase the cycle available specific thrust, as well as potentially enable the use of existing turbojet engines for flight Mach numbers up to 4 or 5.
2. For a given trajectory with a fixed compressor face area and compressor face Mach number, pre-cooling can potentially reduce a vehicle's required specific thrust, by allowing greater mass flow to be ingested into the engine. This statement applies to the ``rubber'' engine, as defined in section 4.2.
3. Required pre-cooler temperature changes for typical missions may be on the order of one hundred to several hundreds of degrees *K*.
4. Required pre-cooler heat transfer rates for a TSTO type mission may be on the order of tens of megawatts.

In what follows, we focus on assessing compressor cooling as an alternative to use of a pre-cooler in SSTJ engine to enable high Mach number flight.

5.0 Compressor Cooling

The temperature-entropy diagram in figure 12 compares standard ideal compression (A-B) to constant pressure pre-cooling (A-C) followed by ideal compression (C-D). The comparison is made on an equal work basis, meaning ΔT is the same for both cases (perfect gas is assumed). As initial temperature increases, two lines of constant-pressure diverge. The salient point of this diagram is that the pressure rise capability of the pre-cooled compressor is greater than the standard compressor, because the work is done at a lower starting temperature.

Figure 13 superimposes a third conceptualization, the case of N constant-pressure cooling steps interspersed with N equal work steps. It is implied by the temperature rise of $\Delta T/N$ that the total work for all three processes (A-B), (A-C-D), (A-E-...-F) is equal. This model could represent: (1) an *N* stage compressor with constant-pressure cooling in each stator, or (2) perhaps, by taking the limit as N approaches infinity, a single stage device with a continuous cooling scheme. Both descriptions will be generally referred to as cooled compressors.
As a component, this cooled compressor underperforms in comparison to a compressor preceded by a lossless constant-pressure pre-cooler, in terms of pressure rise capability per given amount of work and cooling. This is due to the fact that by pre-cooling all of the fluid at constant-pressure first, lines of constant-pressure are as close together as possible on a Temperature-entropy (T-s) diagram, making it easier to raise the stagnation pressure for a given amount of work. This model fails, however, to account for the fact that a real pre-cooler does create significant loss of stagnation pressure. Assuming that a cooled compressor introduces no new gas path geometry, and hence no new loss generating solid boundaries, the cooled compressor underperformance may be mitigated or even reversed when compared to a real pre-cooler[2]

The natural point of departure from this conceptual example is to determine in what situations a cooled compressor may be superior to a compressor with pre-cooling. For example, figure 14 shows the critical pre-cooler recovery factor versus non-dimensional heat addition for the comparison of two compressors with a pressure ratio of 2. The first compressor is cooled by a real pre-cooler with stagnation pressure recovery, π_r, while the second is a one-stage device with

---

[2] In addition to the loss penalties associated with a real pre-cooler, significant system weight penalties from heat exchanger hardware are also seen as a technological challenge, requiring lightweight heat exchanger materials to be surmounted [Powell et al. (1988). In this progress report we do not address the modeling of system weight. It may be necessary in future studies.

50% cooling in the inlet guide vane (IGV) and 50% cooling in the stator. To first order, the presence of compressor cooling is assumed to introduce no new loss mechanisms. The interpretation of this plot is that for a given level of cooling, read off the x-axis, the pre-cooler is superior if π_x is above the line, while the cooled compressor is superior if π_x is below the line. The lower the level of cooling, the higher the critical stagnation pressure recovery for the pre-cooler to be superior to the cooled compressor. In the literature the stagnation pressure loss ($\Delta p_t/p_t$) of a pre-cooler is generally one to eight percent, and is a function of pre-cooler temperature drop [Powell et al. (1988)].

The next step will be to determine the cooling potential of a compressor given the available surface areas for heat exchange and how cooling affects the compressor loading potential and compressor efficiency. To begin we first consider a subsonic stator. We employ a control volume approach to determine the bulk effect of cooling on stator pressure rise. It is assumed that the control volume has uniform velocity, pressure, temperature and density, upstream (u) and downstream (d) of the passage entrance. Upstream conditions are known and based upon the total temperature (T_{tu}) and total pressure (p_{tu}) along the trajectory given in section 3. Upstream Mach number, M_u, is also assumed to be known and subsonic. Furthermore, it is assumed that the upstream flow angle (α_u) and the the downstream flow angle (α_d) are known.

A sample calculation has been made for flight Mach number M_0=4, with upstream and downstream flow angles set to α_u =50° and α_d =25°, respectively. Upstream Mach number is varied. The results from this model show that cooling increases the static pressure rise in the passage, as illustrated by the plot of pressure coefficient versus non-dimensional heat transfer in figure 15. As M_u increases, the effect of cooling is greater, as seen by the relative slopes of the three lines. This result is consistent with the Mach number dependence of the static pressure sensitivity coefficient given in compressible flows texts for quasi one-dimensional flow with heat transfer. Figure 16 shows that cooling also increases the passage stagnation pressure, with heating producing the opposite effect. Again this is consistent with the quasi 1-D, Rayleigh line result. Such a control volume approach can be extended to a rotor, so that a simple cooled compressor model can be built to allow comparison between a single stage (IGV/Rotor/Stator) cooled compressor and an adiabatic compressor preceded by a real pre-cooler for determining under which circumstances the cooled compressor may prove superior to the pre-cooled compressor.

A typical multi-stage axial compressor contains highly three-dimensional flows that must be well characterized in order to control stage matching. To do so one must first extract figures of merits that provide performance characterization (e.g. total pressure change, flow turning, et al) for use in meanline procedure. Here of interest are the implications of new control variables such as cooling rates. To this end, we have thus focused on (1) the effect of cooling in two-dimensional cascade flows, (2) single-stage and multi-stage compressor behavior using cooled two-dimensional cascade results from CFD, and (3) the effect of cooling in a high speed rotor with finite tip clearance gap. The results from the implementation of these tasks are presented next.

5.1 Cooling in Two-Dimensional Cascade Flows

Results from CFD experiments on two-dimensional cascades geometries show that on an area-averaged or mass-averaged basis, the presence of cooling on the surface of a cascade airfoil decreases the total pressure loss coefficient, ω, and also increases the flow turning, $\Delta\beta$, measured as the angle made between the inlet and exit velocity vector (where the exit velocity vector is formed by the mass averaged components of the exit velocity). Both decreased ω and increased $\Delta\beta$ represent performance improvements to two-dimensional cascades. In addition, cooling decreases the blade row exit stagnation temperature, $T_{t,exit}$, and also decreases the blade row exit Mach number, M_{exit}, relative to adiabatic. These last two effects are beneficial to the downstream blade row in an axial compressor.

5.1.1 Two-Dimensional Cascade Results

CFD experiments on 2D cascade flows have been performed to produce loss buckets (non-dimensional total pressure loss vs. incidence at various Mach numbers). Cascade geometry has been selected for the study, based upon a typical cascade airfoil inside an eight stage compressor. The airfoil geometry was based upon the NACA 65 airfoil series blade definition, with an inlet and exit metal angle (based on the leading edge and trailing edge camber line tangency) of α_{in}=38° and α_{out}=0°, respectively. The cascade solidity was chosen to be 0.75.

A large matrix of cases were run by varying upstream total pressure and flow inlet angle, and keeping downstream static pressure fixed. Cases were run both with (1) adiabatic airfoil walls and also (2) a heat flux boundary condition for cooling. The non-dimensional cooling rate is defined as the heat removed from the flow divided by the inlet stagnation enthalpy:

$$q^* = \frac{\dot{Q}}{\dot{m} h_{t,in,\text{blade ref}}} = \frac{\Delta h_t}{h_{t,in,\text{blade ref}}} \tag{11}$$

In this report all of the results for cooled cascades are presented at a non-dimensional cooling rate of q*= -0.001, which, for a perfect gas at 1000K (typical of the first compressor stage in a high flight Mach number power plant) represents a 1K temperature reduction. All of the cooling data points were linearly interpolated to this value of q* from their actual values.

Various integrated bulk flow properties were measured and used as the basis for the cascade performance data shown. For example, upstream conditions such as inlet Mach number, M_{in}, and inlet static and stagnation pressure, p_{in} and $p_{t,in}$, respectively, were measured on a plane one chord length upstream of the leading edge of the airfoil. Downstream conditions such as exit stagnation pressure, and x and y components of the downstream velocity, $u_{av,out}$ and $v_{av,out}$, respectively, were measured one chord length downstream of the trailing edge. The downstream velocities were mass-averaged, while the static and stagnation pressure were area-averaged[3]. All of the results were then linearly interpolated to a given set of Mach numbers in order to produce the loss buckets.

Figure 17 shows adiabatic and cooled loss buckets generated from the 2D CFD experiments. For a given inlet Mach number, there is an incidence value of minimum total pressure loss (``minimum ω incidence"). Positive or negative departures from this minimum ω incidence result in an increased total pressure loss. At low subsonic Mach numbers (M_{in} ~ 0.4), the loss bucket shows a wide range of incidence over which ω remains virtually constant, beyond which ω increases rapidly (due to positive or negative incidence stall). At high subsonic Mach numbers (M_{in} > 0.7) the incidence range near the ``minimum ω loss" neighborhood becomes quite narrow. As total pressure loss coefficient, ω, is defined as change in stagnation pressure between cascade inlet and outlet divided by the inlet dynamic pressure (compressible formulation), the primary effect of cooling is to produce a decrease in ω. At high Mach number, there is an indication that the shape of the loss bucket in the cooled case opens up slightly (i.e, the ``minimum ω" neighborhood becomes wider). In the analysis of section 5.2, results for loss and flow turning (deviation) have been assumed to scale linearly with cooling.

Figure 18 shows the flow turning, $\Delta\beta = \beta_{in} - \beta_{out}$, versus incidence angle at a low and high subsonic Mach number. Flow turning has a nearly straight line behavior over a large range of incidence angles. At high positive incidence, i.e., heavily stalled positive incidence flow, the amount of flow turning appears to level off. At the high subsonic inlet Mach number there is less flow turning than at the low subsonic Mach number. The relationship between incidence, inlet Mach number, and turning is unique to each cascade airfoil geometry and solidity, as evidenced by results for different airfoil geometries [Cumpsty (1989)]. It can be seen that the cooled

[3] It was found that area-averaging of stagnation pressure produced no appreciably different result versus mass-averaging

cascades exhibit a greater amount of flow turning versus adiabatic ones. For example, at low subsonic inlet Mach numbers, (M_{in} ~ 0.4), a cooling rate of q*= -0.001 gives ~ 0.1 degrees of additional turning, and at high subsonic inlet Mach numbers (M_{in} ~ 0.8) the same cooling rate give ~ 0.25 degrees of additional turning. In the axial compressor study in section 5.2, we select cooling rates up to ten times higher (q*= -0.01), giving extrapolated turning values due to cooling of 2-3 degrees in the high Mach number stages of the compressor.

Figure 19 shows an interesting result. It compares the channel flow sensitivity coefficient given in [Shapiro(1953)] (approximated by using the inlet Mach number, M_{in}),

$$\frac{dp_t}{p_t} = -\frac{\gamma M^2}{2}\frac{dT_t}{T_t} \quad \text{or} \quad \left(\frac{dp_t/p_t}{dT_t/T_t}\right) = -\frac{\gamma M^2}{2} \approx -\frac{\gamma M_{in}{}^2}{2} \tag{12}$$

to computed differences between cooled and adiabatic fractional total pressure change, $\left(\frac{dp_{t,cool}}{p_t} - \frac{dp_{t,adiabatic}}{p_t}\right)$, divided by cooled fractional temperature change, $\frac{dT_{t,cool}}{T_t}$. One way to interpret the plot may be that for low subsonic inlet Mach numbers, the channel flow sensitivity coefficient is a good first approximation to the effect of cooling on total pressure change, whereas at high subsonic inlet Mach numbers (e.g., M_{in}>0.8), cooling may have a more beneficial impact above and beyond the bulk cooling of the working fluid.

Figure 20 shows the exit Mach number of the cascades for adiabatic and cooled cases. Although the effect is not great, it is clear that the exit Mach number is lower for a given incidence and inlet Mach number. This is a result that occurs from the mass, momentum and energy balance of the flow subject to bulk reversible cooling. Again, from the sensitivity coefficients for simple one-dimensional channel flow [Shapiro(1953)], we see subsonic cooling has the effect of reducing the Mach number (just as heating does the opposite, driving flow towards sonic conditions):

$$\frac{dM^2}{M^2} = \frac{(1+\gamma M^2)(1+\frac{\gamma-1}{2}M^2)}{1-M^2}\frac{dT_t}{T_t} \tag{13}$$

This effect of a Mach number reduction downstream (in most compressors) will be to reduce the inlet Mach number into the next blade row, having a potentially favorable effect on the loss due to compressible flow effects.

In summary, the effect of cooling is to decrease the value of ω and increase the flow turning, $\Delta\beta$, both of which favorably affect compressor performance. In addition, there is a decrease in the exit stagnation temperature and a slight decrease in the exit Mach number, which may both favorably affect subsequent downstream blade rows, due to the increased pressure rise capability (on an equal shaft work basis) on a relatively colder fluid and the decrease in ω with decreasing Mach number. In the next section we apply these blade surface cooling results to a one-dimensional compressor model.

5.2 Axial Compressor Behavior Using 2D Cooling Results

As use of two-dimensional cascade data represents a first step in determining the performance of a multistage compressor on a meanline basis, results from 2D CFD experiments have been used to assess the effect of cooling on a single stage and an eight stage compressor. As the number of stages is added, the matching of the stages becomes critical. The presence of cooling affects matching significantly, both in terms of the propagation of off-design perturbations to velocity triangles and in terms of total pressure loss. Results show that constant corrected speed lines (constant $N_c = N/\sqrt{T_{t,in}/T_{ref}}$) on a compressor map are raised relative to their adiabatic counterparts. Qualitatively, cooling affects low N_c lines differently than high N_c lines. This is primarily due to the Mach numbers seen by the airfoils at low and high values of N_c. At high

values of N_c (and hence high rotor Mach numbers), there is a very narrow range of incidences for the airfoils to operate successfully in. There is also an increase of loss with increasing Mach number. Cooling (1) increases the pressure rise, (2) increases the turning, (3) decreases the downstream stagnation temperature, and also (4) slightly decreases the downstream Mach number. Effects (2), (3), and (4) all potentially affect the flow conditions into the next cascade in a favorable manner.

5.2.1 Generic Rules for Cascade Loss and Deviation

By introducing cooling to the cascades, we have added one more non-dimensional variable into the cascade performance, namely, the non dimensional cooling, q*. For this study, we assume that cooling takes place at a uniform rate over the airfoil surface. In fact, tailoring of the cooling distributions is also a design variable. However, to make use of this data in a general sense, we wish to simplify our definition so that we may isolate the effect of each variable. The set of variables that describe the cascade performance parameters of interest are then,

$$\textit{Cascade performance} = \textit{function}(\textit{geometry}, i, M_{in}, Re_c, q^*) \tag{14}$$

where,

- *geometry* (including airfoil shape and cascade solidity, σ) is fixed for the experiment.
- i is the inlet flow incidence.
- M_{in} is the inlet Mach number.
- Re_c is the inlet Reynolds Number, using airfoil chord as an appropriate length scale.
- q* is the non-dimensional cooling rate, defined as the ratio of the change in stagnation enthalpy due to cooling to the inlet stagnation enthalpy (see equation 11 and Appendix A). Because cooling involves heat removal, we have adopted a sign convention that q* is always Negative for cooled cascades.

Generic rules for cascade loss and deviation were created by postprocessing the CFD results shown in the previous section. The motivation for using generic rules came from the fact that no detailed geometry information exists during preliminary design of a compressor. These rules serve as a set of trends that can be used in a preliminary compressor design. For the situation where dependence on Re_c is weak[4], and the solidity only appears in the expression for `base' deviation (i.e., Carter's rule[5],
Equation 14 simplifies to:

$$\omega, \Delta\delta = f(i, M_{in}, q^*) \tag{15}$$

where,

- ω is the total pressure loss coefficient.
- $\Delta\delta$ is the change in deviation relative to the `base' deviation (given by Carter's rule).

The generic loss buckets, both adiabatic and cooled (q*=-0.001) are shown in figure 21. These rules were developed by taking each loss bucket (adiabatic and cooled, at given Mach number) from the CFD data and referencing its minimum ω value as `zero' incidence. Polynomial fits were then used to define the bucket in the incidence range of -15° to 15°. The difference in loss between the cooled and adiabatic CFD cases was then taken, and the cooled bucket was linearly

---

[4] For the CFD cases that were run, values of Re_{c} ranged from 100,000 to 200,000. Re_{c} does not change appreciably between comparable adiabatic and cooled cases. At present, we are less interested in absolute levels of loss and more interested in capturing the differences between adiabatic and cooled cases

[5] Carter's rule gives the base deviation (predominantly a potential flow effect) near the minimum ω point, $\delta_{base}=m\theta\sigma^n$, where m is an empirical constant which depends on geometry, θ is the camber angles (angular difference between blade metal inlet tangency and exit tangency) and n is usually taken as 0.5 for decelerating cascades [Cumpsty(1989)]

interpolated to a reference q* value of -0.001. For a high flight Mach number vehicle at high altitude (e.g, $M_{flight} \sim 4$, $h=25$ km), a typical temperature in a compressor might be on the order of 1000K. Thus, the reference value of q* would represent a 0.1 reduction of inlet stagnation enthalpy, or a stagnation temperature change, ΔT_t of approximately 1K (approximating air over small amounts of cooling as a perfect gas). For a low level of cooling (lq*l << 1), the channel flow sensitivity coefficient (which relates a small change in stagnation temperature of a perfect gas to the resultant small change in stagnation pressure) is linear for a given Mach number (equation 12). We assume that to first order, it will be reasonable to scale the change in ω due to cooling linearly with the cooling rate.

Nominal deviation for adiabatic cascades at design (minimum ω) is predicted by using Carter's rule to obtain a nominal value, and then modifying it for incidence, Mach number, and cooling rate using the rules shown in figures 22 and 23. The first deviation modification, $\Delta\delta_{adiabatic}$, shown in figure 22, is the increase in deviation due to `off-design' incidence and Mach number for an adiabatic cascade. The second modification is reduction of deviation due to cooling ($\Delta\delta_{cool}$) as shown in figure 23 (at q*= -0.001). The change in deviation due to cooling has been assumed to vary linearly with the non-dimensional cooling rate. The effect of inlet Mach number on $\Delta\delta_{cool}$ has been included, while the effect of incidence has been neglected by averaging the values of $\Delta\delta_{cool}$ at each Mach number. Cooling at the low subsonic Mach number ($M_{in} \sim 0.4$) gives ~ 0.1 degrees of turning, while at the high subsonic Mach number ($M_{in} \sim 0.8$) give ~ 0.25 degrees of turning for q*= -0.001$. If levels of cooling several times higher are available (q* ~ -0.01), two to three degrees of deviation may be recoverable from the blade rows at high subsonic Mach numbers. Two to three degrees of deviation reduction per blade row could make cooling a legitimate control variable to improve off design matching.

5.2.2 On- and Off- Design Constant Radius Meanline Analysis

A meanline analysis has been used to design an eight stage compressor and apply the aforementioned loss and deviation rules to produce compressor maps for an adiabatic and a cooled compressor. The hub and tip radii were chosen so as to keep the meanline radius constant from blade row to blade row. The first stage of the eight stage design has also been studied as a single stage.

The eight stage compressor is designed by specifying compressor inlet conditions based upon a flight vehicle at 25 km altitude and flight Mach number of 4, assuming that a lossless inlet exists upstream of the compressor. The overall pressure ratio at design is taken as 5, with each stage producing the same pressure rise. Air is assumed to behave as a perfect gas with γ=1.4. The compressor is sized for a `typical' high flight Mach number vehicle by specifying an inlet corrected flow[6] of 51 kg/s. The meridional layout of the eight stage compressor is shown in figure 24. The layout of the first stage is shown in figure 25. The results from the first stage alone are presented in subsection 5.2.3. Results from the eight stage device are presented in subsection 5.2.4.

5.2.3 Effect of Cooling on Single Stage Fan

Results from 2D cascade studies were applied to both a single stage and a multistage analysis. The single stage fan map comparing an adiabatic and a cooled fan stage is shown in figure 26. We introduce a new non-dimensional compressor cooling variable, q', which relates the cooling in each blade row to the compressor face inlet stagnation enthalpy (a discussion of the use of q* and q' is included in Appendix A):

---

[6] $\dot{m}_c = \dfrac{\dot{m}\sqrt{T_t/T_{ref}}}{p_t/p_{ref}}$, where T_{ref} and p_{ref} are standard day conditions.

$$q' = \frac{\dot{Q}}{\dot{m} h_{t,in,\text{compressor face}}} = \frac{\Delta h_t}{h_{t,in,\text{compressor face}}} \tag{16}$$

For a non-dimensional cooling value of q'= -0.01, results indicate that the constant corrected speed line on a given compressor map (pressure ratio vs. corrected mass flow) moves up and to the right[7]. This means that a cooled compressor produces a greater pressure rise at a given corrected mass flow and corrected speed. This also implies that as corrected mass flow increases along a given corrected speed line and as the speed line approaches vertical on the compressor map (i.e. choked), a cooled compressor can pass greater corrected mass flow versus an adiabatic compressor. The increase in corrected mass flow occurs both at high and low corrected speed, but a constant value of q' affects the corrected speed lines differently. For example, at high corrected speed (100% N_c) the `stall' side of the speed line shows a greater improvement in pressure ratio for the same corrected mass flow, than at low corrected speed (60% N_c). Examination of the one-dimensional flow properties given in the table in Appendix B explains why this is so. The table shows inlet and exit Mach numbers, incidences, changes in deviation (relative to Carter's rule), and total pressure loss coefficients for the rotor and stator blade rows. The improvement in pressure ratio on the high speed line is primarily due to the rapid increase in loss with increasing Mach number, and the narrow range of operable incidences at high Mach numbers. The 100% N_c line is in the high subsonic regime, where, cooling has a more pronounced impact on loss and deviation versus the low subsonic regime that is encountered along the 60% N_c line. Comparing the stator inlet and exit Mach numbers of points *c* (adiabatic) and *d* (cooled) shows that in the adiabatic case the stator behaves as a throttle, and is no longer diffusing the flow, whereas in the cooled case there is much less total pressure loss and the stator is still diffusing the flow. The difference in stator incidence varies by only 2.4 degrees, but since the inlet Mach number is in the high subsonic regime, the loss in the cooled stator is 50 %, lower than the adiabatic stator. Comparing these two points to their low N_c counterparts, points *g* and *h*, shows that the smaller reduction in total pressure loss due to cooling comes from less incidence change and lower inlet Mach numbers. Points *e* and *f* shows even less change, as their Mach numbers are closer to the low subsonic regime.

Studies on the single stage fan reveal that the improvement in pressure rise capability seen on the compressor map is attributable to both the increase in stagnation pressure from cooling (lower ω) and the increased flow turning. Figure 27 shows the change in cooled speed lines when the effects on total pressure loss and flow turning are both isolated, and when they are both included. The plot shows that both of these effects appear comparable when isolated and applied alone.

The corresponding efficiency map for the single stage compressor is shown in figure 28. Here we have chosen to define the efficiency as follows:

Adiabatic efficiency:

$$\eta_c = \frac{\dot{m} c_p \left(T_{t_{d,s}} - T_{t_u}\right)}{\dot{m} c_p \left(T_{t_d} - T_{t_u}\right)} = \frac{\pi^{(\gamma-1)/\gamma} - 1}{\tau - 1} \qquad \left(\pi = \left[T_{t_{d,s}}/T_{t_u}\right]^{\gamma/(\gamma-1)} \;;\; \tau = T_{t_d}/T_{t_u}\right)$$

$$= \frac{\text{"isentropic (ideal) work for given pressure ratio } (\pi)\text{"}}{\text{"actual work"}}$$

Efficiency with cooling:

$$\eta_c = \frac{\dot{m} c_p \left(T_{t_{d,s}} - T_{t_u}\right)}{\dot{m} c_p \left(T_{t_d} - T_{t_u}\right) - \dot{Q}} = \frac{\pi^{(\gamma-1)/\gamma} - 1}{\tau - 1 - q'} \qquad \left(q' = \frac{\dot{Q}}{\dot{m} c_p T_{t_u}}\right)$$

$$= \frac{\text{"isentropic (ideal) work for given pressure ratio } (\pi)\text{"}}{\text{"actual work"}}$$

[7] It should be noted that the chosen value of q' in both the single stage and multi-stage examples leads to values of q* which require extrapolation of the two-dimensional cascade data presented in section 5.2.1

The computed change in efficiency with and without cooling is approximately 2 to 2.5 points for q`=-0.0025.

5.2.4 Effect of Cooling on Eight Stage Compressor

Four different cases were analyzed on a hypothetical eight stage compressor using the meanline design framework. The compressor map for an adiabatic case and three cooled cases is shown in figure 29a. The cooling schemes, as indicated in figure 29b, are q'=-0.0025 in all eight stages (rotor & stator cooling), q'=-0.01 in the first two stages, and q'= -0.01 in the last two stages. The three cooling rates are non-dimensionally equivalent, so that for a given corrected mass flow, the same cooling rate in units of power (e.g. Watts) applies.

It is worthwhile to first consider the operating environments of the six adiabatic points, *i* through *n*, shown in figure 29a. Points *i, j*, and *k* are on the high speed (100% N_c) line, and represent the design point, a high speed `stall side' point and a high speed `choke side' point, respectively. Points *l*, *m*, and *n* are on the low speed (60% N_c) line, and represent a point having the same throttle characteristic as point *i* (i.e., a low speed throttle point), a low speed `stall side' point, and a low speed `choke side' point, respectively. The tables in Appendix C show the incidence angles and inlet Mach numbers into the eight rotors and stators for these points, which set the levels of ω and $\Delta\beta$. From the tables, it is clear that the adiabatic design point, *i*, has zero incidence into each rotor and stator. The Mach number into the rotors is above 0.8 in the early stages[8], i.e. in the high subsonic regime. As one moves along the speed line towards the `stall side', i.e, in the direction of decreasing corrected mass flow, all of the rotor and stator incidences increase (point *j*) monotonically. In the opposite direction, towards point *k*, all of the blade row incidences {\em decrease} monotonically. At low power, the low speed throttle point, point *l*, shows that the front stages are all operating at positive incidence, while the rear stages all operate towards negative incidence. The change in incidence from stage to stage progresses monotonically from `stall' side to `choke' side. Again, moving along the low speed line in the direction of lower mass flow increases the incidence on all blade rows, while moving in the opposite direction has the opposite effect.

Again referring to the table, the inlet Mach numbers from stage to stage reveal an important compressor characteristic. On the 100% N_c line Mach numbers primarily decrease from front to back, while on the 60% N_c line they increase. This is due to the fact that the annulus areas at low N_c are `under-designed' to pass the required mass flow, versus at high N_c. Stated another way, at low speed the front stages provide relatively less charging pressure (or density rise) to pass the required mass flow leading to greater axial (and blade relative) Mach numbers. The degree to which the annular area is `under-designed' on the low $N_c$ line increases as the rear stages are reached. From the compressor map we see, therefore, that cooling in the last two stages alone has greater effect on the `choke side' of the low N_c line than on the `choke side' of the high N_c line.

The compressor map also clearly shows that at all corrected speeds for the cooling schemes presented, the best pressure ratio is achieved by (1) cooling the first two stages, followed by (2) cooling all stages, (3) cooling the last two stages, and finally (4) the adiabatic case. This is consistent with the result which says that ideally, a lossless pre-cooler is superior to cooled compression}, because the fluid upon which shaft work is being done is at the lowest temperature possible, producing the best total pressure rise. It is well known that at low N_c the rear of the compressor sets the mass flow capability. Moving along a low N_c speed line in the direction of increasing $\dot{m}_c$, the front stages provide lower and lower pressure (or density) rise, leading to

---

[8] Note that this represents an area of extrapolation in the generic loss bucket data, as M_{in}=0.8 is the maximum Mach number included in the generic loss buckets and flow turning data. We expect consistency in the cooling performance trends beyond the range of data shown (up to `higher' subsonic Mach numbers such as M_{in} ~ 0.9), because we extrapolate using data from lower subsonic Mach numbers into a region where there is typically a strong divergence of flow properties (e.g., drag, pressure coefficient), therefore making our extrapolations conservative. We also expect this diverging trend to apply to changes in cascade performance due to cooling. For example, equation 12 tells us that the incremental total pressure reduction goes up parabolically with increasing Mach number for `small' amounts of cooling.

higher and higher axial velocities in order to pass the required mass flow in the rear stages. The rearmost stator thus encounters flow at larger negative incidences, leading to higher losses, and reduced turning capability. Eventually, turning is reduced to such low amounts that throttle-like behavior sets into the rearmost stator, increasing the compressor exit Mach number until it reaches the thermal choking limit of 1. Since putting all of the cooling in the first two stages produces the largest increase in corrected mass flow at all speeds, we may conclude that the presence of cooling in upstream blade rows relieves the adiabatic choking limit in the downstream rows. This effect arises both due to the increased pressure (or density) rise capabilty in the cooled upstream blade rows, and the temperature reduction (relative to adiabatic) into the downstream blade rows.

We present in Figure 30 a representative cooled compressor map with the corresponding cooled efficiency versus corrected mass flow obtained using the meanline procedure developed here. The efficiency gain can be as much as 6 points.

5.3 Results for Cooled High-speed Transonic Rotor

In this section we present some preliminary results from a cooled high-speed rotor to contrast against the corresponding adiabatic results. The rotor geometry is based on the NASA Stage 35 transonic rotor design. The grid being used was provided by Dr. Rod Chima of NASA. This grid has been imported into GAMBIT and modified for use with FLUENT. Shown in Figure 31a is the computational domain while figure 31b shows the temperature on the surfaces of the flow path indicating that cooling is imposed on blade surfaces, tip casing and hub surface.. Three-dimensional Reynolds Averaged Navier-Stokes computations of Stage 35 rotor have been implemented for adiabatic and non-adiabatic (cooled) situation. The computed compressor pressure rise characteristic for adiabatic and cooled Stage 35 rotor at 93.7 percent corrected speed is shown in Figure 32. In accord with the results from the meanline compressor analysis based on computed cascade data information, the cooled Stage 35 rotor has a higher pressure rise and a larger mass flow capacity. As indicated in figure 32, the computed results appear to be in line with the measurements under (near) adiabatic operations. As of this writing we have not computed the corresponding efficiency as well as determined the response of rotor tip clearance/endwall flow to imposed cooling.

6.0 Summary

In summary we first began by recognizing the need to quantify the potential for turbomachinery-based airbreathing propulsion systems to achieve wide flight Mach number operating ranges. A survey of selected previous work indicates that numerous concepts have been studied in the past, including many combined cycle and pre-cooled compressor concepts. Within the context of realizing wide flight Mach number operating ranges using available technology, the concept of a pre-cooled turbojet engine appears to be a viable candidate. An ideal cycle study was performed for the case of the pre-cooled SSTJ. We deduce from this study the following:

- Pre-cooling can potentially increase the cycle available specific thrust, as well as potentially enable the use of existing turbojet engines for flight Mach numbers up to 4 or 5.

- For a given trajectory with a fixed compressor face area and compressor face Mach number, pre-cooling can potentially reduce a vehicle's required specific thrust, by allowing greater mass flow to be ingested into the engine. This statement applies to the ``rubber'' engine, as defined in Section 3.0.
- Required pre-cooler temperature changes for typical missions may be on the order of one hundred to several hundreds of degrees K.

- Required pre-cooler heat transfer rates for a TSTO type mission may be on the order of tens of megawatts.

Generally, it is recognized that there are potential cycle benefits associated with enhancing compressive shaft work by cooling. This naturally includes cooling which takes place inside the compressor component itself, a concept which has received little or no attention to the author's knowledge. Analysis shows that an ideal pre-cooled turbojet will outperform an ideal cooled compressor, but that real losses in a pre-cooler (as well as system weight penalties) may create situations in which a cooled compressor may be a superior candidate. It is also believed that cooling in a compressor may add a degree of freedom to control of the three-dimensional aerodynamics inside the static and rotating blade passages, which may have an impact on operability.

It is noted that

- For a fixed polytropic efficiency, a given amount of shaft work can achieve a greater pressure rise on a low tempeature fluid (at the same initial pressure) than on a high temperature fluid (i.e., lines of constant pressure diverge on a T-s diagram as T increases).

- Cooling a fluid increases its density, allowing the turbomachine to pass a greater mass flow.

- Aerodynamic benefits such as reduced boundary layer growth may result from cooling at a wall.

We have used two-dimensional computational flow experiments on cascade geometry to produce total pressure loss and flow turning maps for adiabatic and cooled cascades. We have applied these maps to an off-design meanline compressor analysis to produce compressor maps (pressure ratio vs. corrected mass flow), for adiabatic and cooled compressors. From our analysis,
we deduce that relative to the adiabatic case, cooling via the blade surface increases a ompressor's pressure rise and mass flow capability, having potential benefits to a turbojet cycle used in a high flight Mach number vehicle. We further deduce that in a multi-stage compressor, cooling in a particular compressor blade row has beneficial effects that are also felt in the downstream stages, leading to a broadening of operability limits. Our modeling indicates that compressor performance improvements come from four effects at the cascade airfoil level:

- The reduction of the total pressure loss coefficient, ω, in the blade reference frame.

- The increase in flow turning, $\Delta\beta$, achievable by the blade row.

- The decrease in stagnation temperature into the following airfoil row, thereby requiring less work on the fluid to achieve a given stagnation pressure rise (assuming no change in process efficiency).

- The decrease in exit Mach number (relative to adiabatic) of the flow in the cooled airfoil row, thereby potentially decreasing the inlet Mach number into the next airfoil row and reducing total pressure loss due to compressibility effects.

To recap, we have now addressed the effect that compressor cooling has on multistage compressor matching; specifically, it is found that an appropriate choice of cooling distribution (among the compressor stages) would unchoke the stages that may be close to choking. An implication on turbo-accelerator operation is as follows: as the turbo-accelerator increases in flight Mach number, it encounters a high recovery temperature, which could lead to a situation

where the rear stages are choked. Use of compressor cooling would serve to unchoke these rear stages, and hence overcome operability difficulties.

7.0 Future Work

We wish to address the high level research question of whether cooling inside an axial compressor provides a realizable benefit to a wide flight Mach number vehicle, such as a a two-stage-to-orbit (TSTO) launch vehicle or a high-speed interceptor, because we see a cooled compressor as a potential way to stretch the flight Mach operating envelope of a turbomachinery-based power plant. We identified several technical issues that need to be addressed in order to determine whether the flight Mach operating envelope for such a power plant can be stretched. These issues were:

- The operational/parametric space in which use of turbomachinery is advantageous over other high flight Mach number propulsion configurations.

- The {\em design characteristics} of high flight Mach number turbomachinery components, which, for the applications considered must require a wide operating range on the compressor map.

- The turbomachinery cooling requirements and the technology barriers that need to be crossed for its implementation.

- The flow phenomena that control and limit the operation of such turbomachinery in the high flight Mach number ranges, including the effect of cooling distribution pattern on blade aerodynamics.

- The operability characteristics of the compressor when subjected to inlet distortion.

The work and results presented in this report have, to a certain extent, addressed the first item by performing system level analysis on a single spool turbojet cycle with and without precooling, to determine where the current turbomachinery operational/parametric space lies and how much it could be changed by cooling (pre-cooling). We have also identified potential component level benefits to cooled compression using results from two-dimensional flow effects, and applying them to a one-dimensional off-design compressor model. With the off-design compressor model framework in place, we have a framework with which we can assess the performance changes to a compressor when cooling is present.

Future work will focus both on inclusion of three-dimensional flow effects (e.g., tip clearance/endwall flows), and determining whether the cooling rates required for significant impact to a high flight Mach number vehicle are achievable. In the near term, CFD results from the three-dimensional flow solutions will be post-processed to extract performance metrics for implementing meanline analysis of single and multistage compressor. In the longer term, the research tasks will focus on identifying the major thermal management technology barriers and how they affect the design of the vehicle/propulsion system. Some of the potential tasks may include:

- Modeling the effectiveness of typical heat sinks (such as conventional and cryogenic fuels) and performing a system level analysis based on the use of (thermodynamic) availibility to compare various cooling schemes (i.e., answering the question of what constitutes the system benefit).
- A comparative study of non-ideal pre-cooling versus compressor cooling, to determine the operating environments in which each is the better candidate.

- Identifying what the design implications (e.g., geometry) are for cooled compressor blades, versus conventional adiabatic blades, in order to achieve the necessary cooling rates.

- Performing a vehicle system weight analysis to determine the weight penalties associated with a cooling system.

- Quantifying the additional thermal management costs to cool a compressor over those which may already exist in a high flight Mach number vehicle that uses thermal management elsewhere on board.

Appendix A

Use of Cooled vs. Adiabatic Performance Data in Compressor Map generation

The non-dimensional cooling rates, q* and q' are used extensively throughout this report. It is important to note that q* is used to characterize cooled cascade performance, while q' is used for cooled compressor performance. The variable q* is used as a means of relating the heat removal in the cascade to the cascade inlet stagnation enthalpy. In presenting cascade performance results,
any q* associated with loss buckets or turning/deviation rules is non-dimensionalized by the cascade's inlet stagnation enthalpy. In presenting compressor performance results, any q' is non-dimensionalized by the compressor face inlet stagnation enthalpy. The meanline analysis model uses the energy equation at constant radius in the blade frame of reference:

$$\dot{m}h_{t,in,\text{blade ref}} + \dot{Q} = \dot{m}h_{t,out,\text{blade ref}} \tag{17}$$

For the compressor maps shown, we have chosen to present constant speed lines for cooled compressors using the q' definition, namely,

$$q' = \frac{\dot{Q}}{\dot{h}_{t,in,\text{compressor face}}} \tag{18}$$

Therefore, the energy equation that the meanline analysis model uses to obtain the exit stagnation enthalpy in the blade relative frame is:

$$\dot{m}h_{t,in,\text{blade ref}} + \dot{m}q'h_{t,in,\text{compressor face}} = \dot{m}h_{t,out,\text{blade ref}} \tag{19}$$

In order to determine the cascade performance due to cooling, we must read the generic loss buckets and turning/deviation data for cooling using the appropriate q*. This is obtained by setting the dimensional heat removal rates equal between equations 11 and 16, to get

$$q^* = q' \frac{h_{t,in,\text{compressor face}}}{h_{t,in,\text{blade ref}}} \tag{20}$$

By convention, q* and q' are negative for cooling.

Appendix B

Single Stage Compressor Data Table

	$M_{in,R}$	$M_{in,S}$	$M_{out,R}$	$M_{out,S}$	i_R	i_S	$\Delta\delta_R$	$\Delta\delta_S$	ω_R	ω_S
Point a	0.9406	0.7184	0.7721	0.6686	0.0000	0.0000	0.3695	0.0449	0.1774	0.0985
Point b	0.9406	0.7005	0.7690	0.6450	0.0000	1.5589	0.3695	0.2998	0.1660	0.0961
Point c	0.9846	0.8310	0.8453	0.9486	-1.9186	-5.7722	1.3819	3.1864	0.2057	0.1871
Point d	0.9846	0.7934	0.8280	0.7700	-1.9186	-3.3720	1.3819	1.0128	0.1911	0.1250
Point e	0.5368	0.4377	0.4684	0.4234	0.9671	-0.7035	0.0003	-0.2287	0.0507	0.0497
Point f	0.5368	0.4358	0.4689	0.4210	0.9671	-0.3111	0.0003	-0.1776	0.0479	0.0464
Point g	0.6635	0.6557	0.6379	0.7180	-7.9626	-14.6605	0.2399	1.7431	0.1106	0.2197
Point h	0.6635	0.6479	0.6343	0.6926	-7.9626	-13.8773	0.2399	1.3474	0.1005	0.1849

Appendix C

Single Stage Compressor Data Table

Incidence	Rotor 1	Rotor 2	Rotor 3	Rotor 4	Rotor 5	Rotor 6	Rotor 7	Rotor 8
Point i	0.0000	0.0000	0.0000	0.0000	0.0000	0.0000	0.0000	0.0000
Point j	3.3324	3.6442	4.1383	4.4836	4.8173	5.2293	5.5084	5.6631
Point k	-0.2097	-0.4085	-0.6961	-1.1128	-1.6910	-2.4472	-3.6143	-5.9669
Point l	10.5388	7.4956	5.4964	3.4352	1.2787	-0.9611	-3.3631	-6.0298
Point m	13.5992	10.2648	8.3033	6.3204	4.2768	2.2005	0.0497	-2.2070
Point n	7.4644	4.7133	2.6315	0.4295	-1.9495	-4.5478	-7.5961	-11.8839

Incidence	Stator 1	Stator 2	Stator 3	Stator 4	Stator 5	Stator 6	Stator 7	Stator 8
Point i	0.0000	0.0000	0.0000	0.0000	0.0000	0.0000	0.0000	0.0000
Point j	4.0006	4.9063	5.4896	6.0675	6.6514	6.8889	6.9234	6.8122
Point k	-0.4601	-0.8030	-1.2734	-1.9292	-2.8011	-4.0118	-6.0137	-11.1650
Point l	11.4098	8.7220	5.7735	2.8070	-0.1267	-3.0388	-5.9945	9.1598
Point m	15.3439	12.7401	9.7965	6.8446	3.9387	1.1226	-1.6238	-4.3324
Point n	7.5027	4.6982	1.6877	-1.3901	-4.4981	-7.8008	-11.7203	-19.1780

M_{in}	Rotor 1	Rotor 2	Rotor 3	Rotor 4	Rotor 5	Rotor 6	Rotor 7	Rotor 8
Point i	0.9406	0.8977	0.8595	0.8250	0.7935	0.7641	0.7367	0.7111
Point j	0.8759	0.8181	0.7730	0.7356	0.7017	0.6696	0.6426	0.6193
Point k	0.9451	0.9062	0.8741	0.8477	0.8270	0.8110	0.8030	0.8118
Point l	0.4573	0.4530	0.4645	0.4787	0.4955	0.5150	0.5384	0.5680
Point m	0.4392	0.4283	0.4373	0.4486	0.4617	0.4766	0.4936	0.5134
Point n	0.4786	0.4813	0.4962	0.5146	0.5373	0.5654	0.6034	0.6672

M_{in}	Stator 1	Stator 2	Stator 3	Stator 4	Stator 5	Stator 6	Stator 7	Stator 8
Point i	0.7753	0.7452	0.7194	0.6972	0.6795	0.6630	0.6483	0.6354
Point j	0.7082	0.6718	0.6416	0.6173	0.5978	0.5802	0.5661	0.5551
Point k	0.7808	0.7551	0.7353	0.7213	0.7140	0.7122	0.7211	0.7672
Point l	0.3825	0.3941	0.4075	0.4244	0.4460	0.4713	0.5024	0.5425
Point m	0.3633	0.3729	0.3833	0.3964	0.4134	0.4328	0.4555	0.4825
Point n	0.4056	0.4201	0.4376	0.4600	0.4891	0.5261	0.5791	0.6885

8.0 References

Anderson, J. D., 1989, *Introduction to Flight, 3rd Ed.* MCGraw-Hill Publishing Company,New York, NY.

Cumpsty, N.A., 1989, *Compressor Aerodynamics*, Longman Group UK Limited, London

Heiser. W. H., Pratt, D., "Hypersonic Airbreathing Propulsion, " AIAA, Washington, DC, 1994.

Hewitt, F.A., Johnson, M. C., "Propulsion System Performance And Integration For High Mach Air Breathing Flight, " High Speed Flight Propulsion Systems, 1991, AIAA Progress in Aeronautics and Astronautics.

Johnson, J. E., "Variable cycle engine developments, " Developments in High-Speed-Vehicle Propulsion Systems, 1995, AIAA Progress in Aeronautics and Astronautics.

Kerrebrock, J. L., 1992, *Aircraft Engines and Gas Turbine, 2nd Ed.*, MIT Press, Cambridge, MA.

Miele, A., 1962, *Flight Mechanics, Volume 1: Theory of Flight Paths*, Addison-Wesley Publishing Company, Reading, MA.

Powell, T.H., Glickstein, M. R., 1988, "Precooled turbojet engine cycle for high mach number applications, " AIAA-88-2946, AIAA/SAE/ASME/ASEE 24th Joint Propulsion Conference.

Rudakov, A. S., Balepin, V. V., 1991, "Propulsion systems with air precooling for aerospaceplane, " SAE Paper 911182.

Shapiro, A. H., 1953, *The Dynamics and Thermodynamics of Compressible Fluid Flow*. Ronald Press, New York.

Sreenath, A. V., 1961, "Studies of turbojet engines for hypersonic propulsion, " Technical report, McGill University, Department of Mechanical Engineering.

This page is intentionally left empty

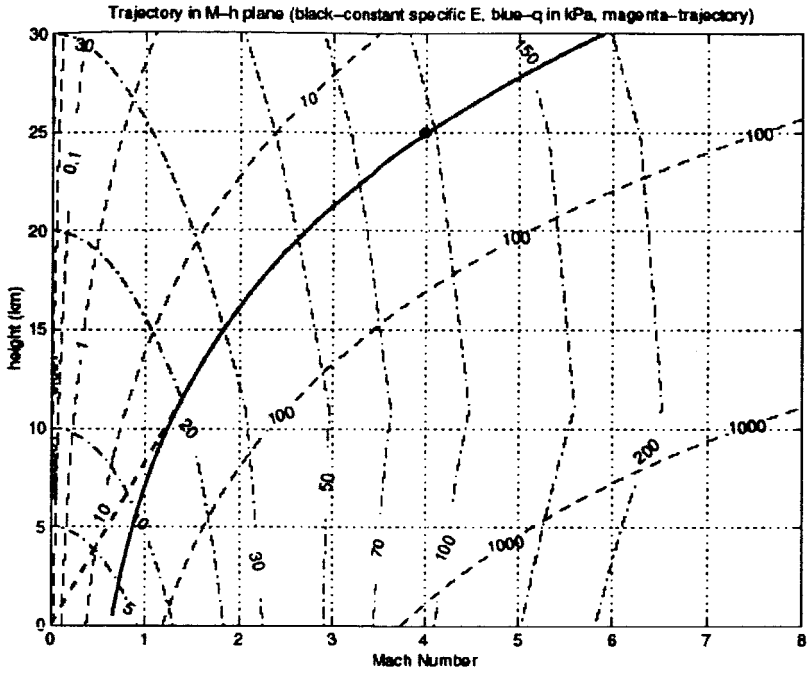

Figure 1: Selected flight path. Heavy, broken line represents low Mach number trajectory. Heavy, solid line is q=0.28 atm, representing high Mach number trajectory. Faint broken lines are lines of constant q in KPa. Faint dash-dot lines are lines of constant specific energy, in km.

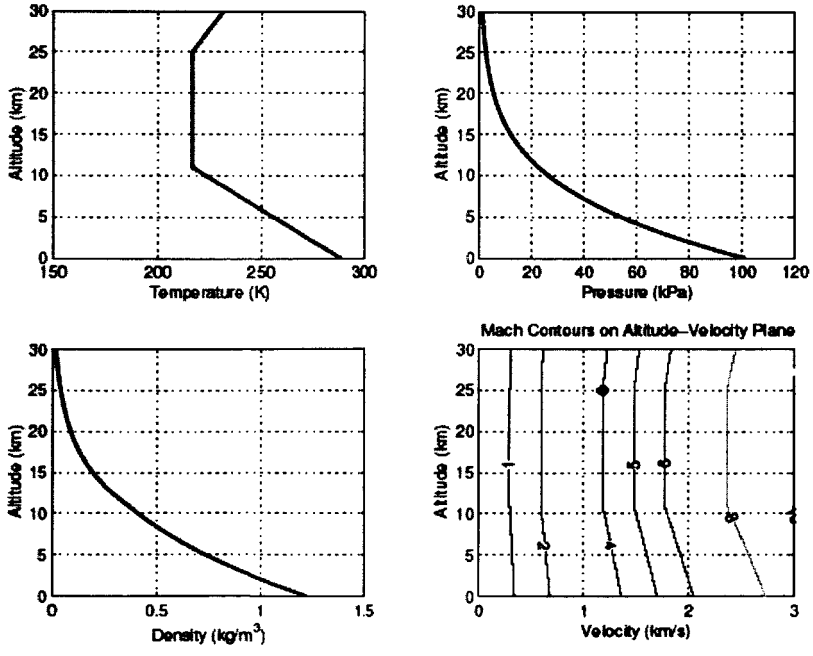

Figure 2: Standard atmosphere model showing temperature, pressure, density, versus altitude, and contours of Mach number in the altitude-velocity plane.

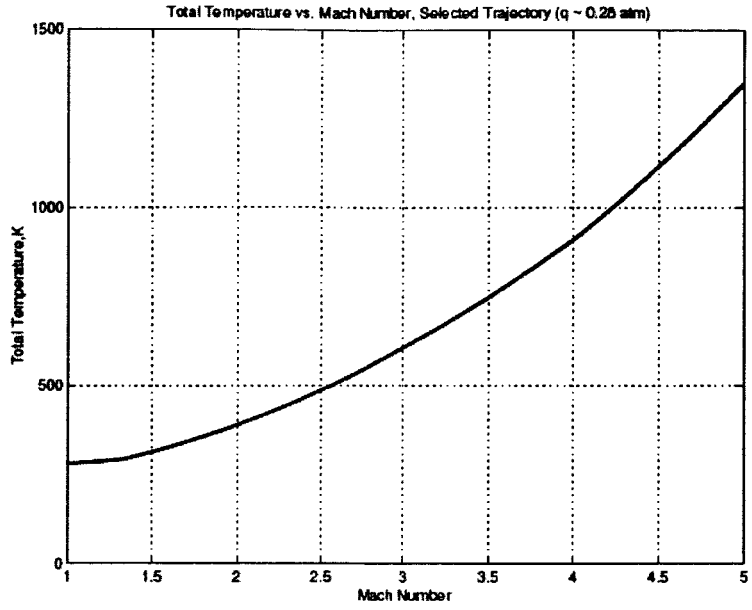

Figure 3: Total temperature versus Mach number along selected flight path.

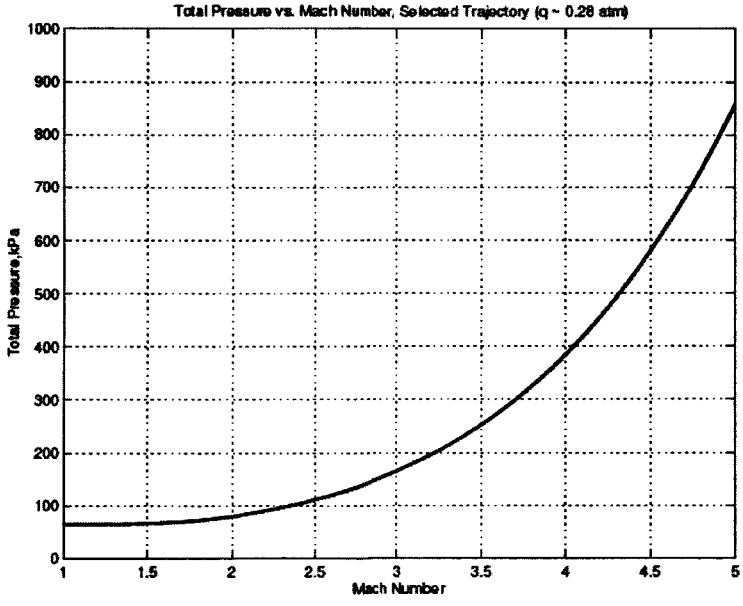

Figure 4: Total pressure versus Mach number along selected flight path

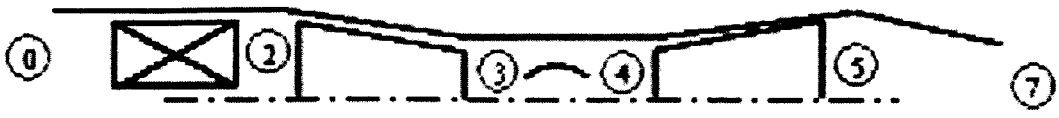

Figure 5: Schematic of SSTJ with lossless, constant-pressure pre-cooling

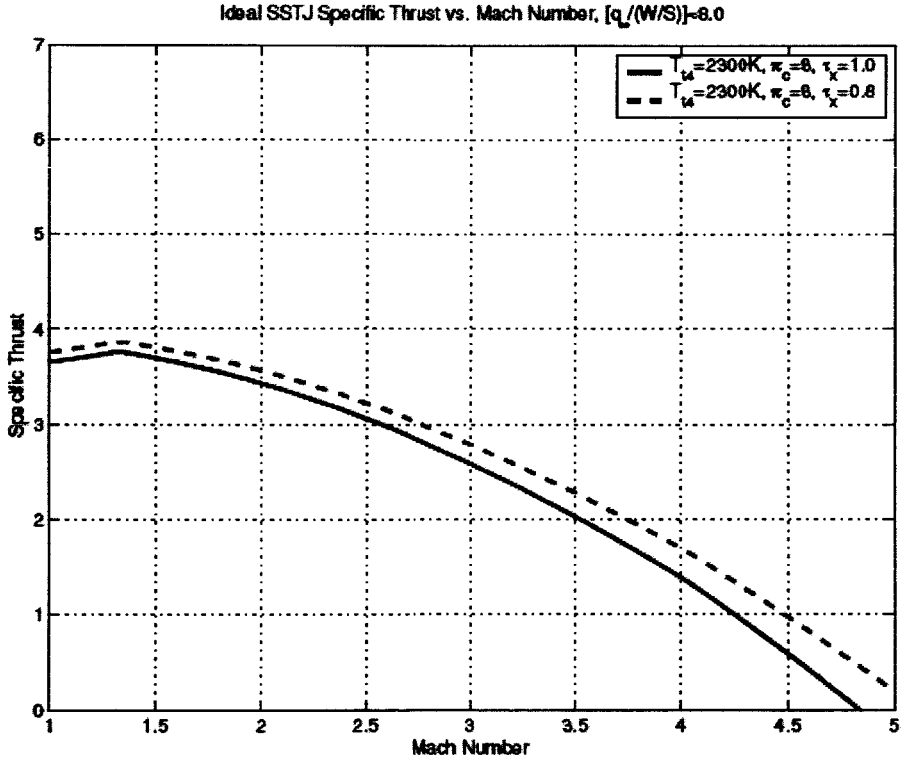

Figure 6: Specific thrust for ideal SSTJ (solid line) and ideal SSTJ with precooling (broken line) for given mission.

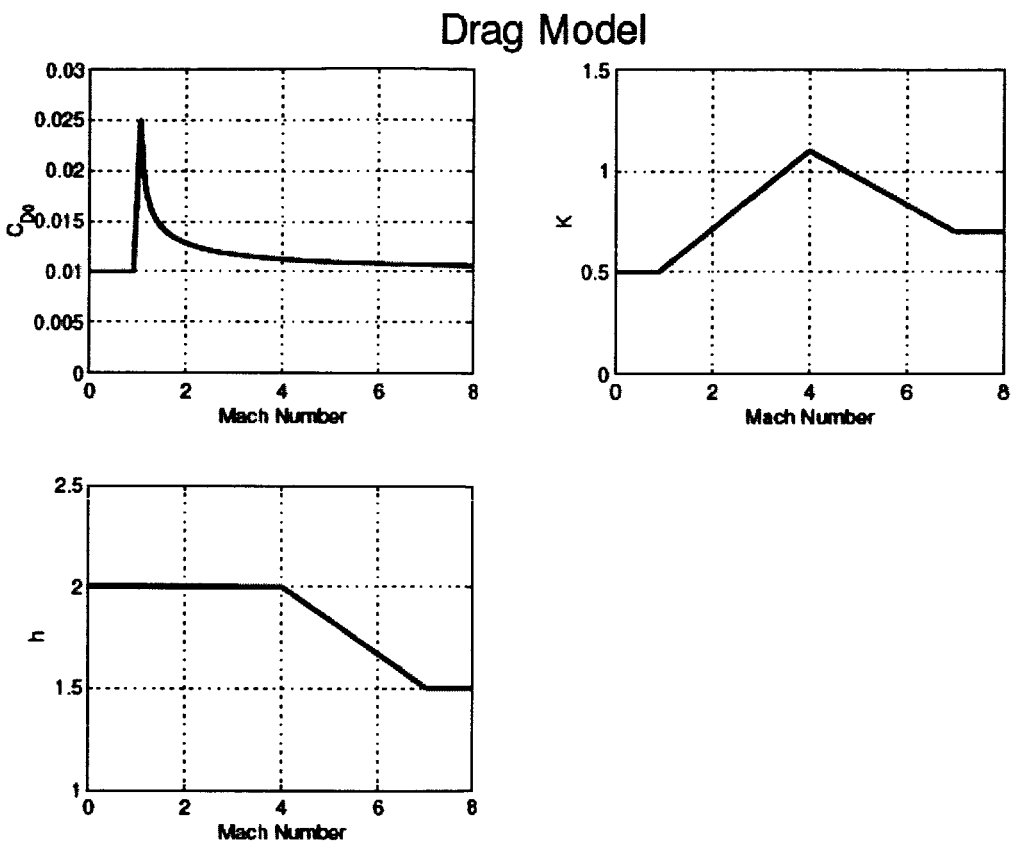

Figure 7: Drag model used in mission analysis

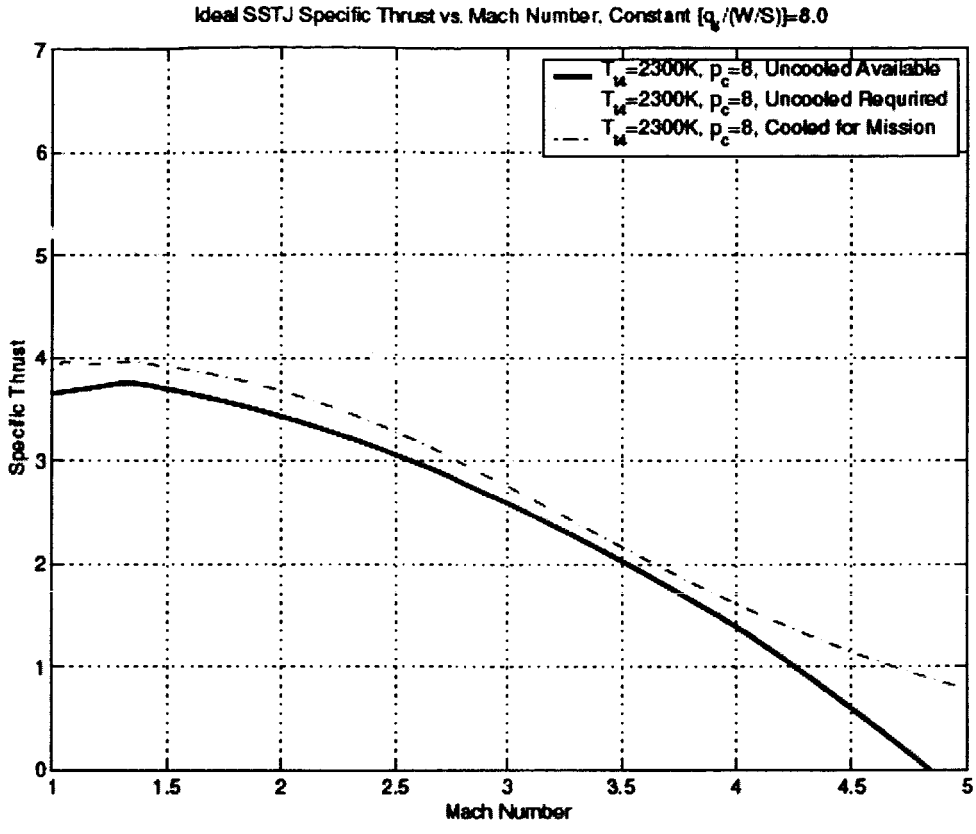

Figure 8: Uncooled available (solid), uncooled required (broken line), and pre-cooled (dash-dot line) specific thrust versus Mach number for chosen vehicle in steady, level flight on selected trajectory.

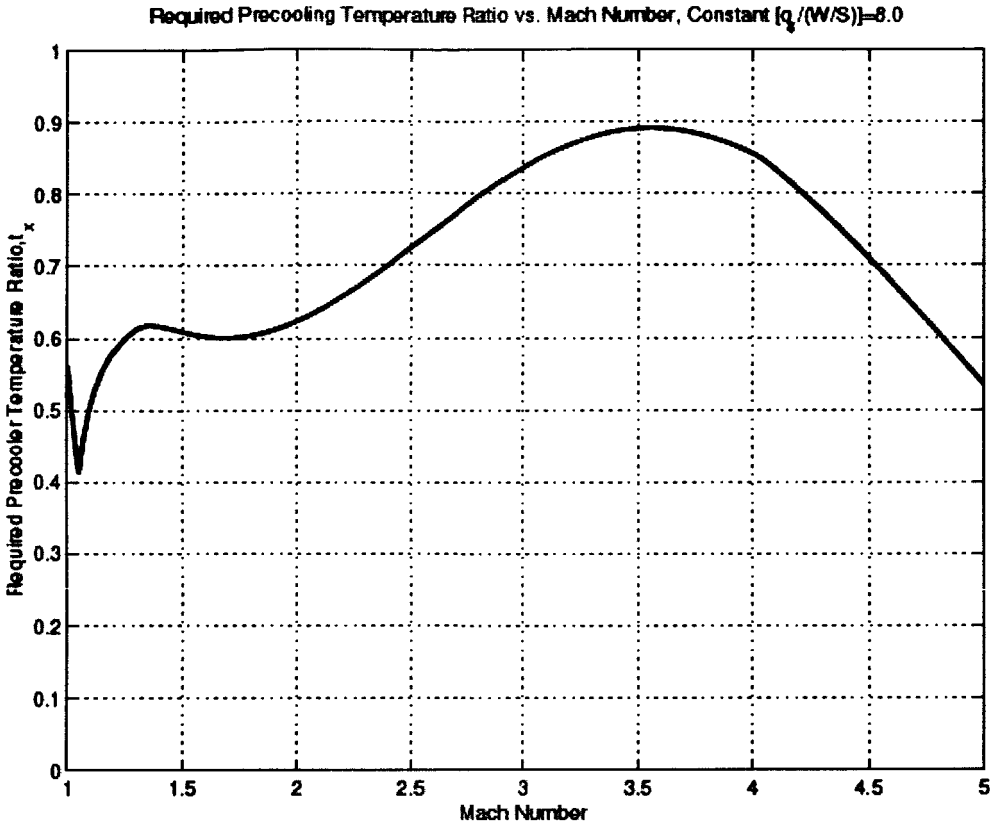

Figure 9: Pre-cooling temperature ratio for chosen vehicle in steady, level flight on selected trajectory

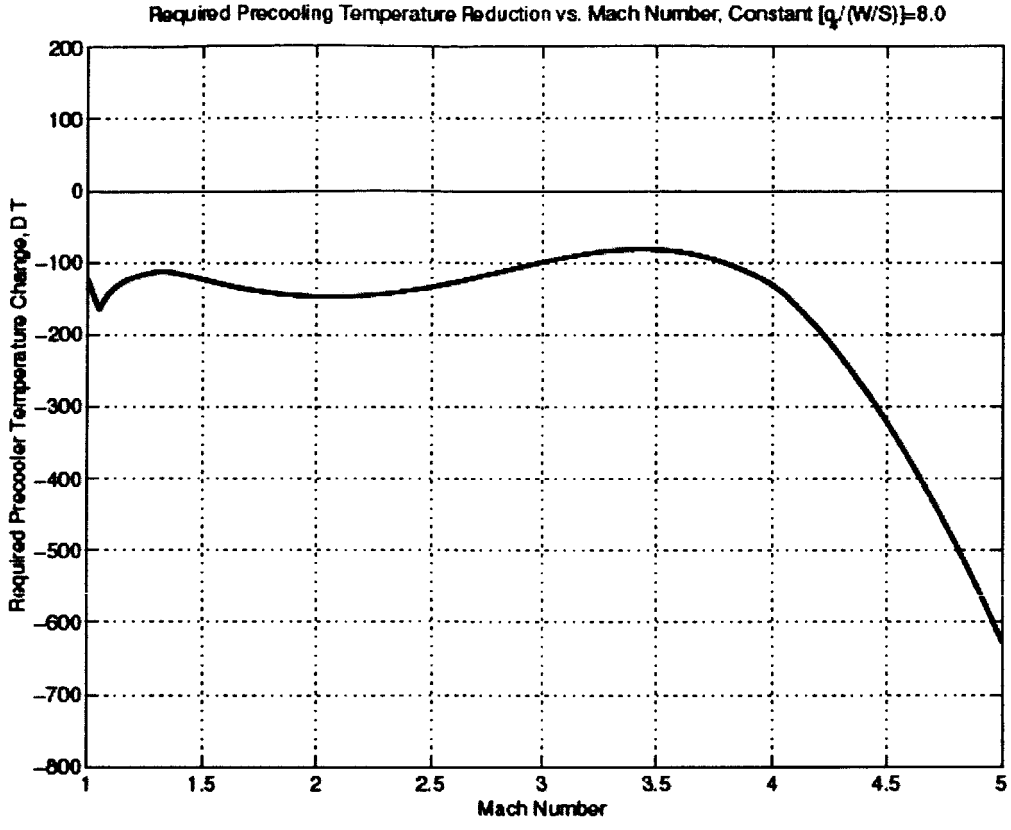

Figure 10: Pre-cooler temperature change (K) for chosen vehicle in steady, level flight on selected trajectory.

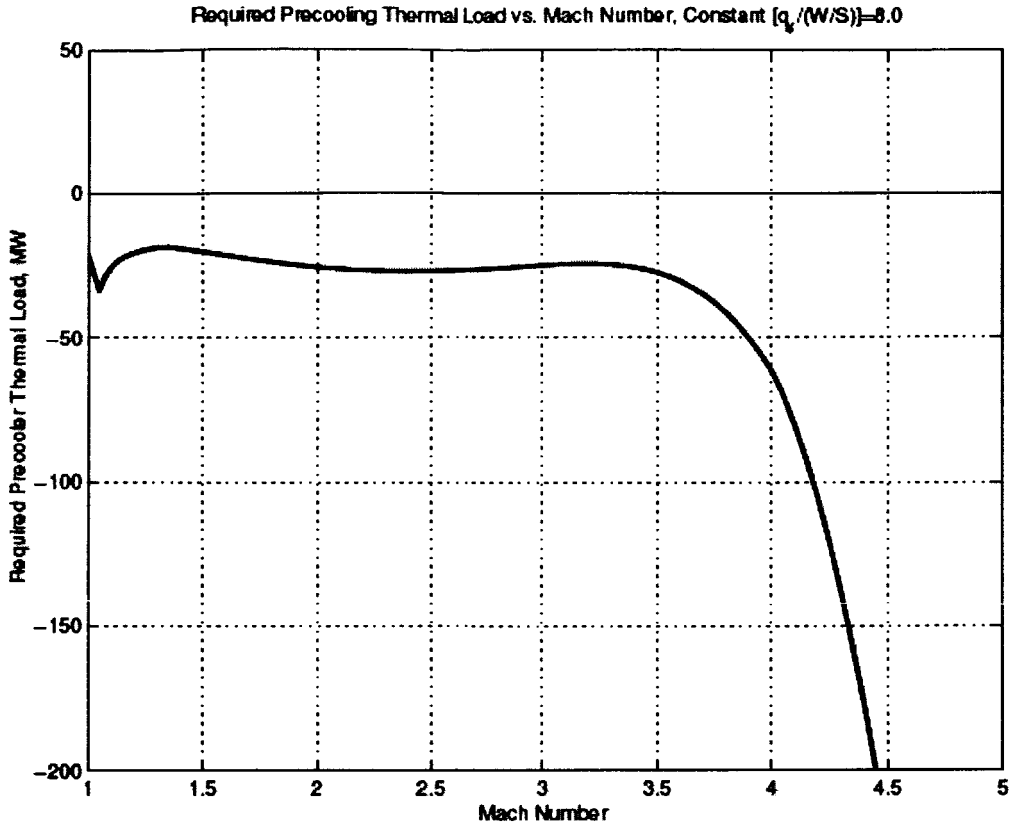

Figure 11: Pre-cooling load (MW) for chosen vehicle in steady level flight on selected trajectory.

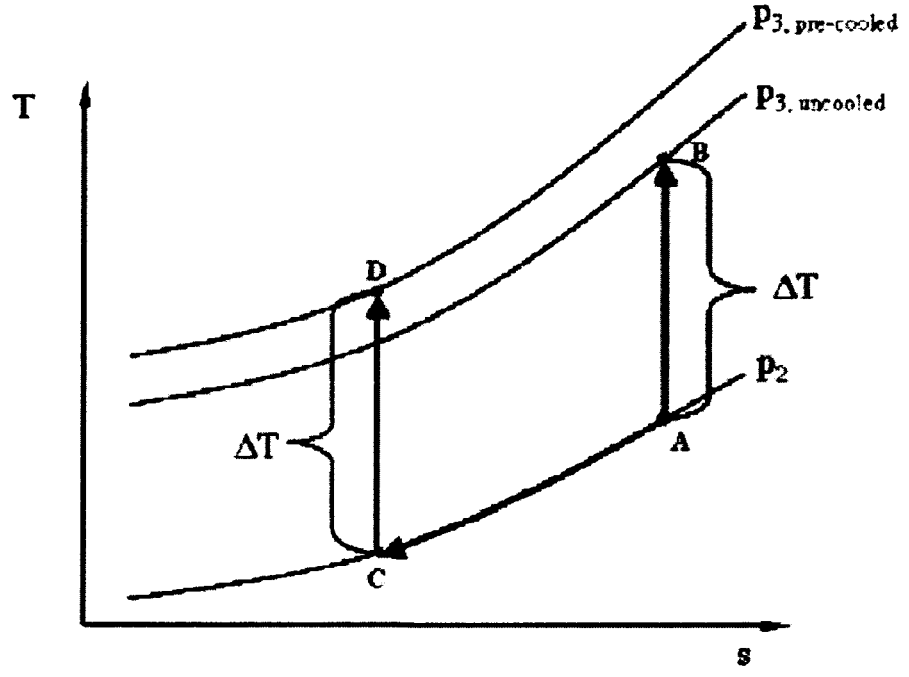

Figure 12: Temperature T, versus entropy, s for standard compression (A-B) versus compression with pre-cooling (A-C-D).

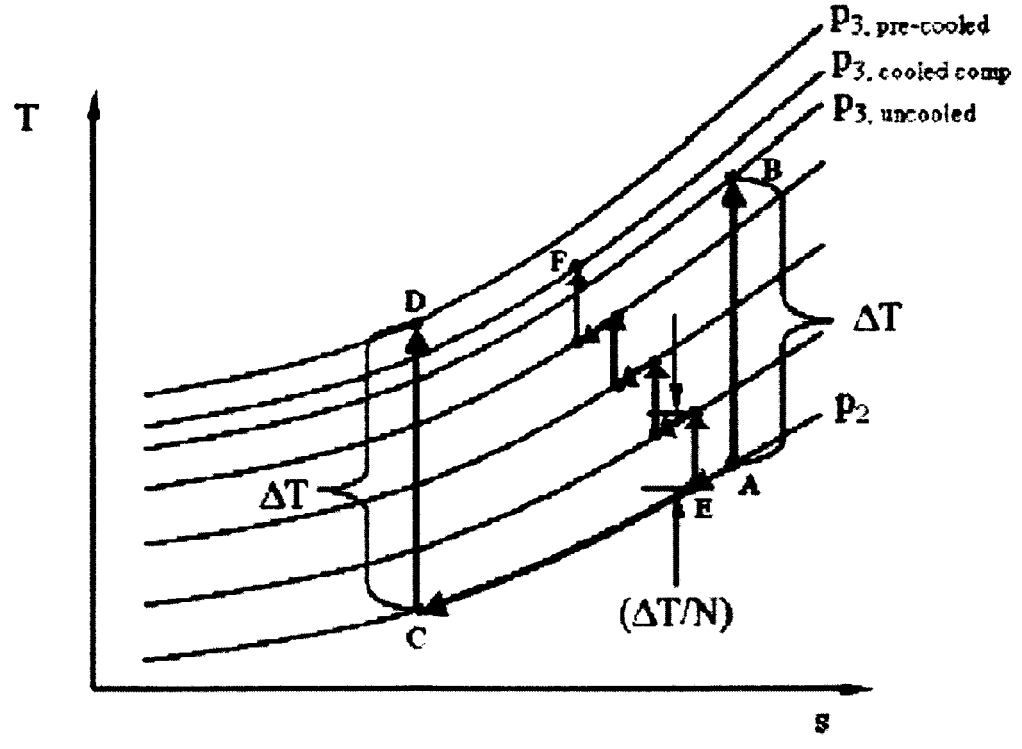

Figure 13: Temperature, T, versus entropy, s for standard compression (A-B), compression with pre-cooling (A-C-D), and interspersed cooling and compression in N steps (A-E_....-F).

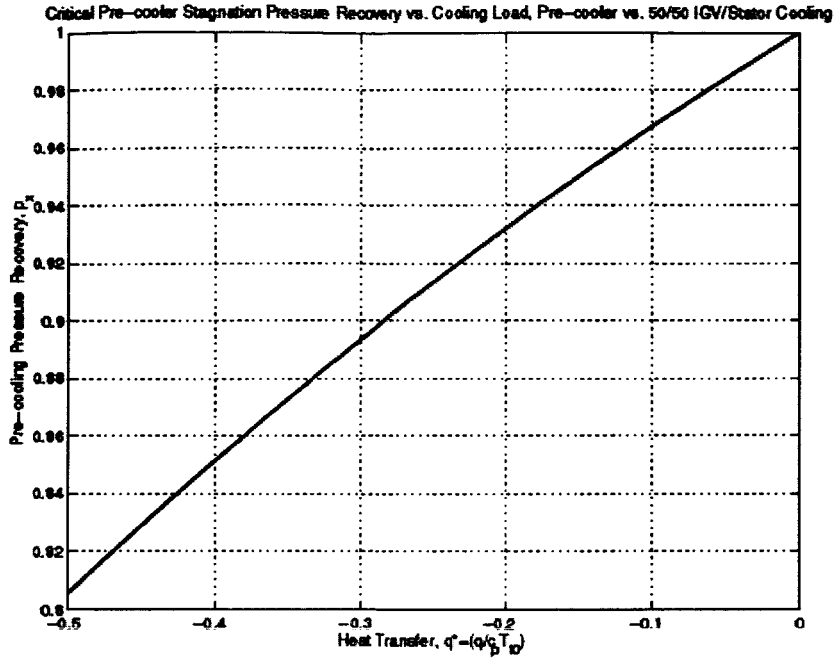

Figure 14: Critical pre-cooling stagnation pressure recovery versus cooling load. Operation above the line favors pre-cooling, while operation below the line favors the 1-stage compressor with 50% cooling in IGV and 50% in stator. Plot is made on an equal work, equal cooling basis.

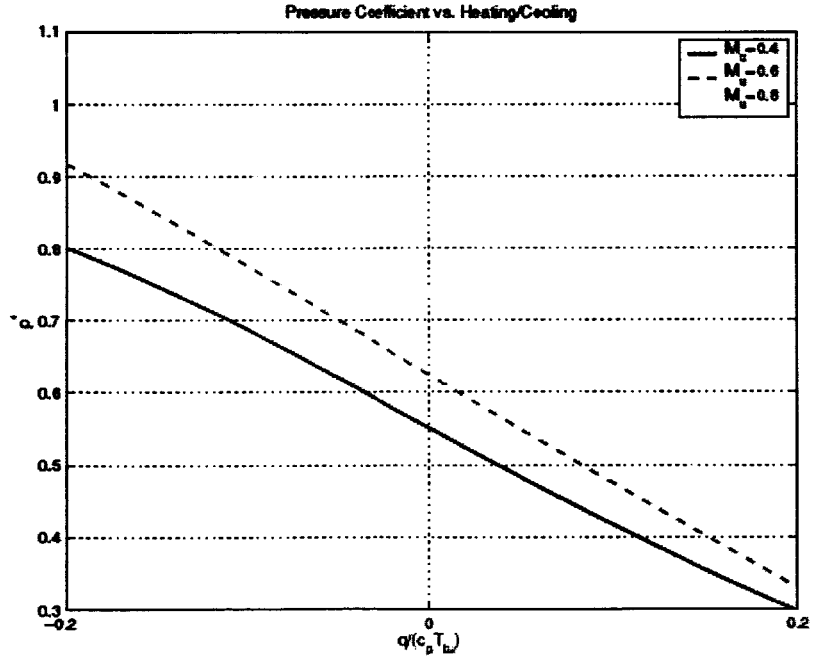

Figure 15: Pressure coefficient, $p^* = \dfrac{(p_d - p_u)}{\frac{1}{2}\rho_u V_u^2}$, versus heating/cooling, $\pm\dfrac{q}{c_p T_{tu}}$ in selected stator passage, at various upstream Mach numbers.

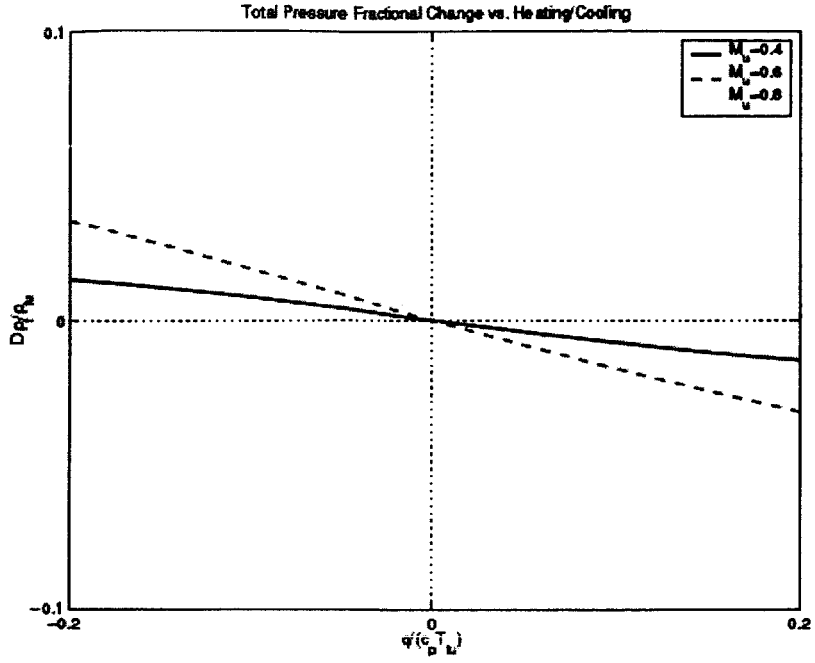

Figure 16: Fractional change in stagnation pressure, $\frac{p_{td} - p_{tu}}{p_{tu}}$, versus heating/cooling, $\pm \frac{q}{c_p T_{tu}}$ in selected stator passage, at various upstream Mach numbers

$$\omega = \frac{p_{t,in} - p_{t,out}}{p_{t,in} - p_{in}}$$

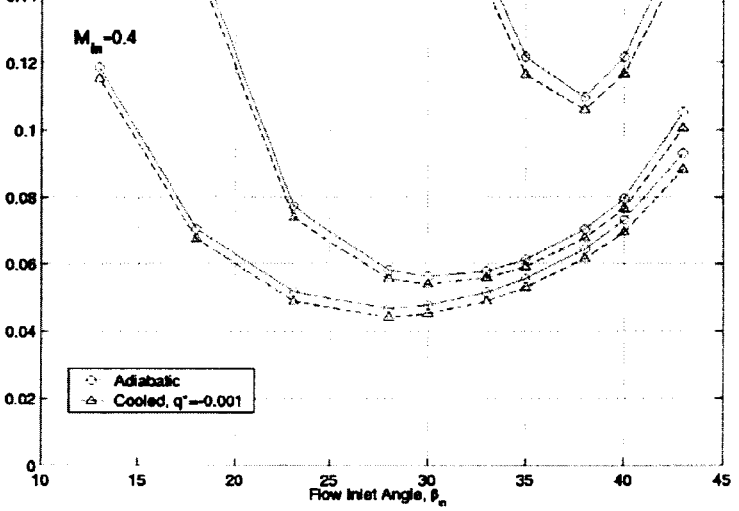

Figure 17: Adiabatic versus cooled loss buckets for selected two-dimensional cascade. Solid line with circles represents adiabatic boundary conditions; dashed line with triangles represents blade surface cooling. Non-dimensional cooling rate q*=-0.001.

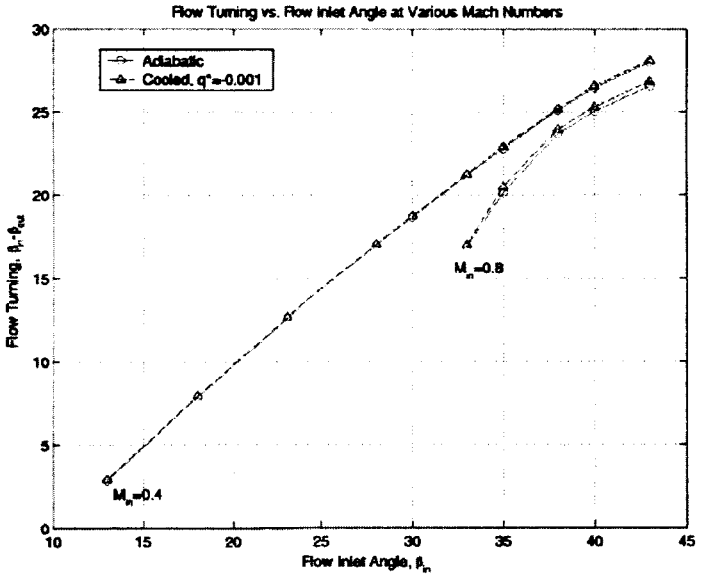

Figure 18: Adiabatic versus cooled flow turning, $\Delta\beta$, for selected two-dimensional cascade. Solid line with circles represents adiabatic boundary conditions; dashed line with triangles represents blade surface cooling. Non-dimensional cooling rate is q*=-0.001

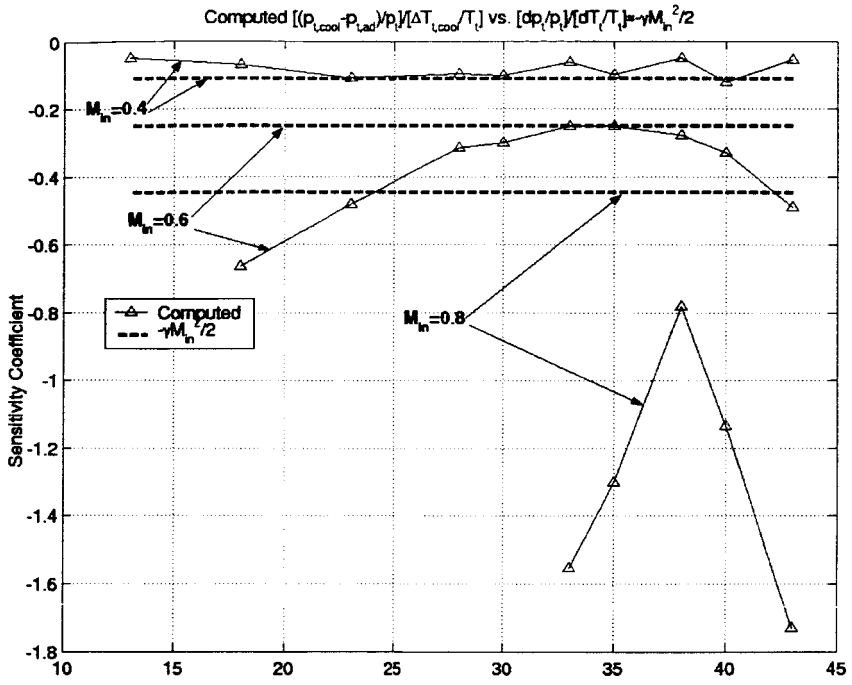

Figure 19: Computed (from CFD) value of $\frac{\left(\frac{dp_{t,cool}}{p_t} - \frac{dp_{t,adiabatic}}{p_t}\right)}{\frac{dT_{t,cool}}{T_t}}$ versus channel flow sensitivity coefficient, $-\frac{\gamma M_{in}^2}{2}$ (at inlet), for selected two-dimensional cascade. Solid line with triangles represents values measured from CFD; heavy dashed line is calculated for M_{in}. Non-dimensional cooling rate is q*=-0.001.

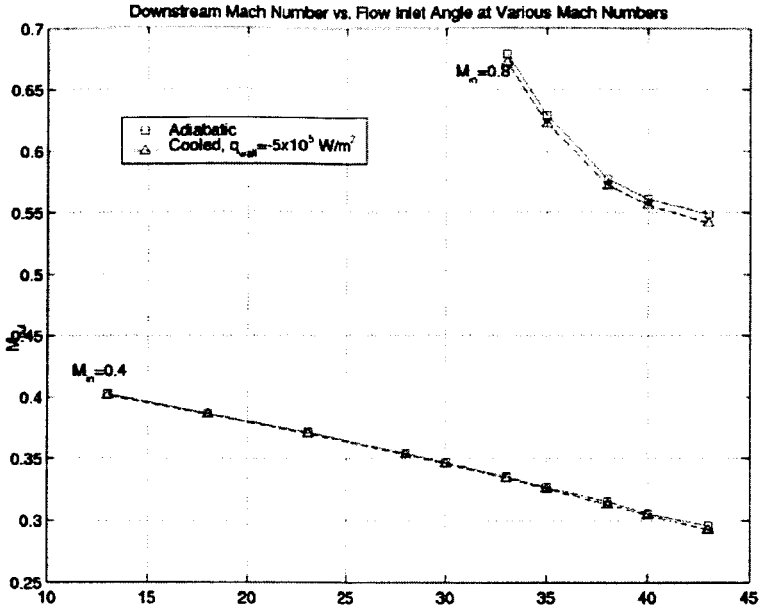

Figure 20: Adiabatic versus cooled exit Mach number, M_{out}, for selected two-dimensional cascade. Solid line with circles represents adiabatic boundary conditions; dashed line with triangles represents blade surface cooling. Non-dimensional cooling rate q*=-0.001.

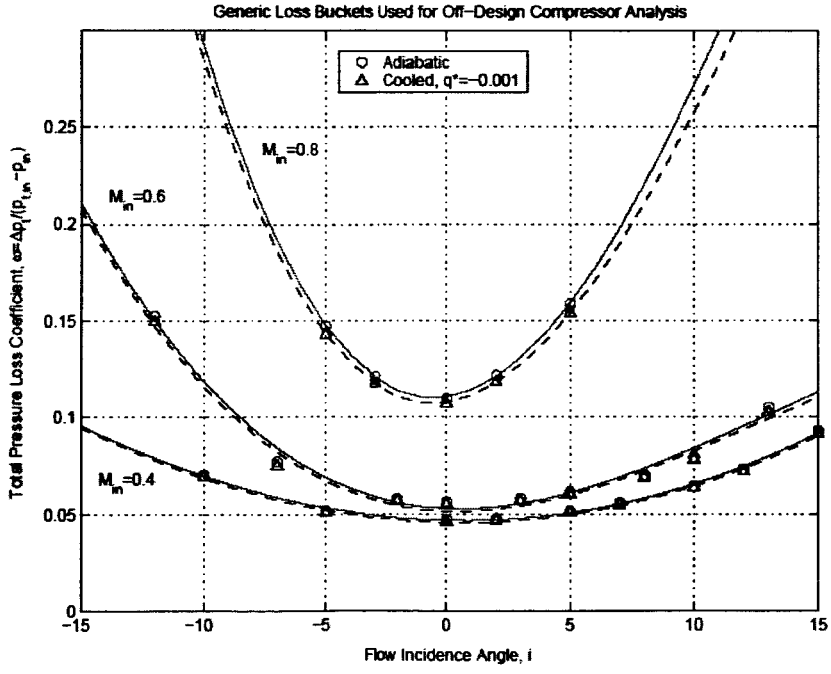

Figure 21: General adiabatic versus cooled loss buckets for selected two-dimensional cascade. Solid line with circles represents adiabatic boundary conditions; dashed line with triangles represents blade surface cooling. Non-dimensional cooling rate q*=-0.001.

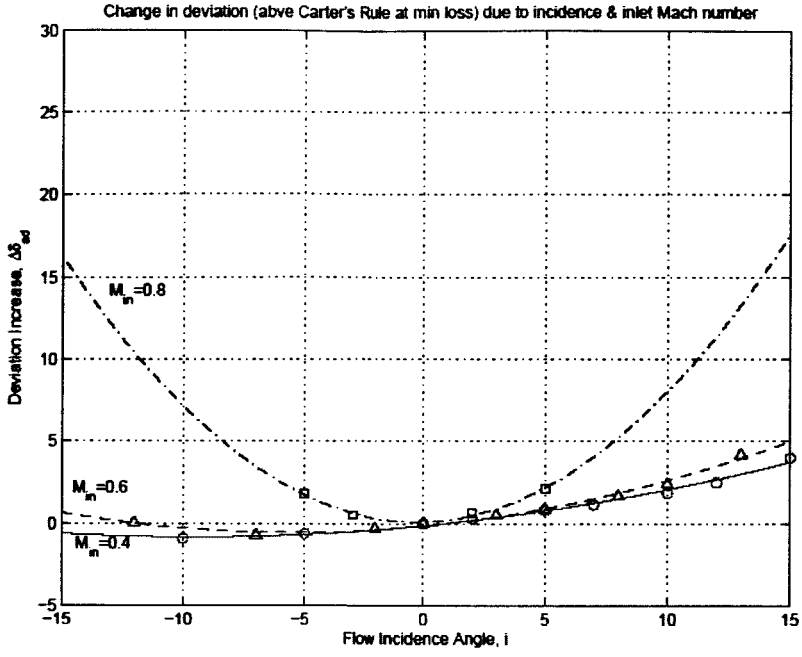

Figure 22: Adiabatic change in deviation, $\Delta\delta$, (relative to Carter's rule) for selected tow-dimensional cascade.

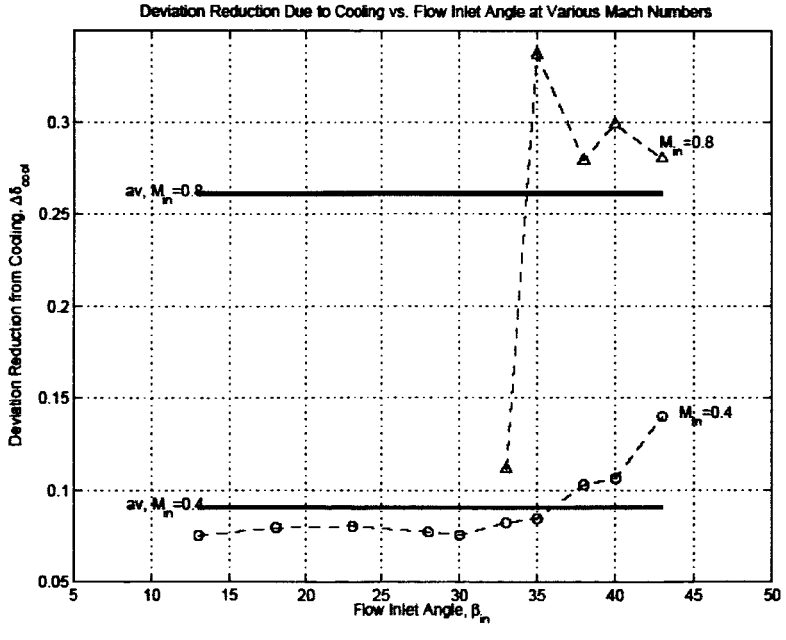

Figure 23: Additional flow turning from cooling, $\Delta\beta cool = -\Delta\delta cool$, for selected two-dimensional cascade. Dotted lines with symbols are CFD results. Heavy solid lines are average values (used in meanline analysis) for given inlet Mach numbers.

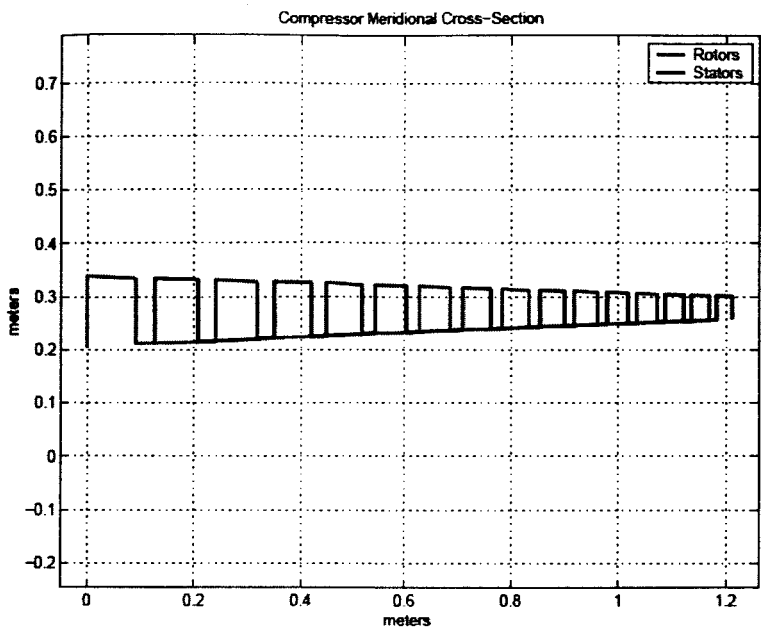

Figure 24: Meridional layout of eight stage compressor. Rotor layout is in red, stator layout is in black.

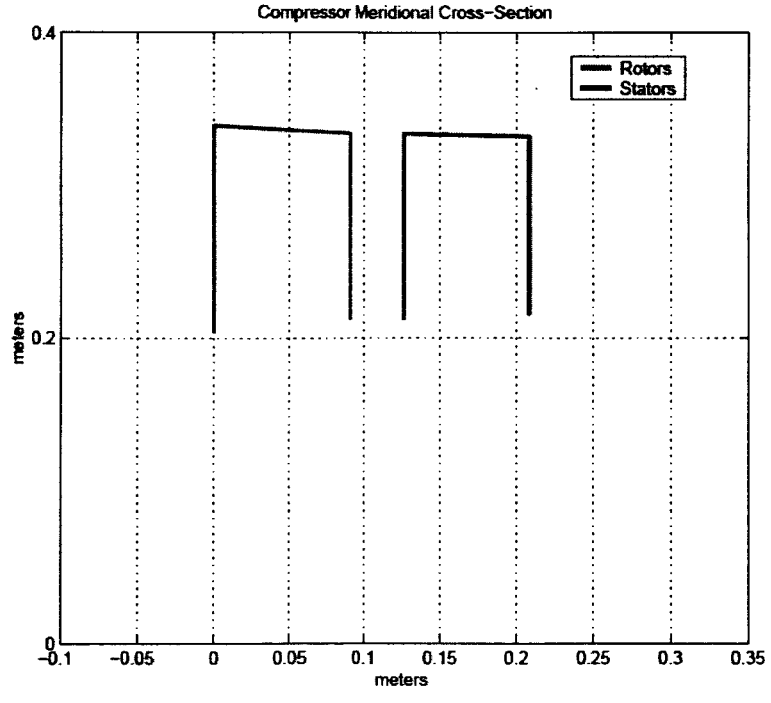

Figure 25: Meridional layout first stage of eight stage compressor, used in single stage analysis. Rotor layout is in red, stator layout is in black.

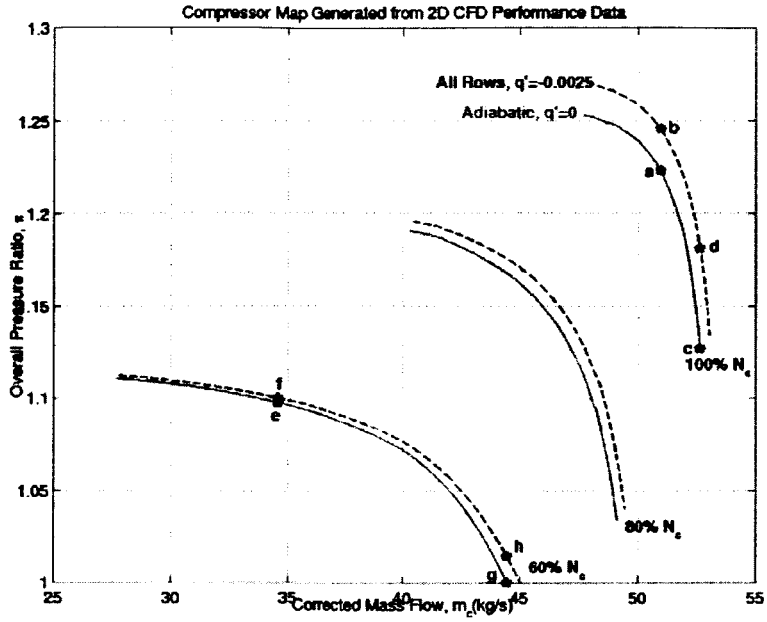

Figure 26: Single stage compressor map, with and without cooling. Solid line is adiabatic; Dashed line is q`=-0.001. 100%, 80%, and 60% N_c lines are shown.

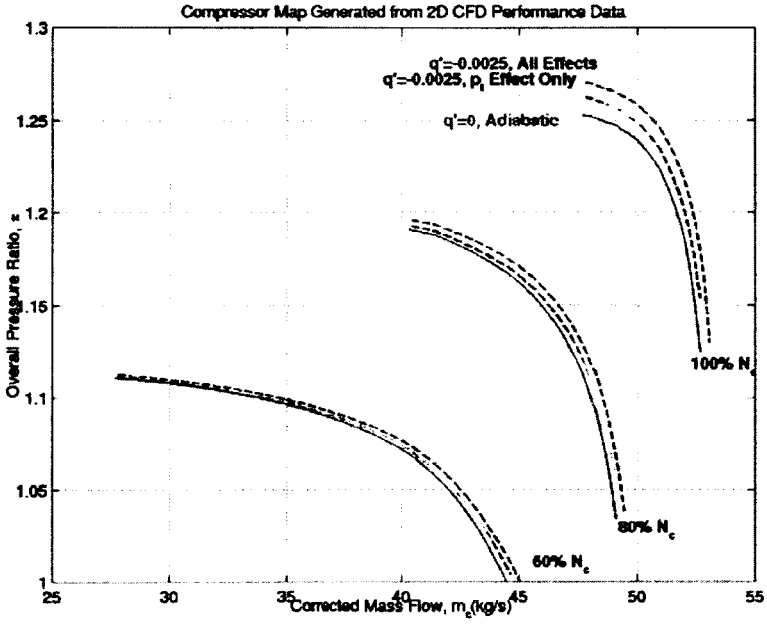

Figure 27: Single stage compressor map, with and without different effects from cooled cascade performance. Solid red line is adiabatic; solid green line shows cooling effects of change in deviation only; dashed black line shows cooling effects of change in ω only; dashed blue line shows both effects. 100%, 80%, and 60% N_c lines are shown. q`=-0.001

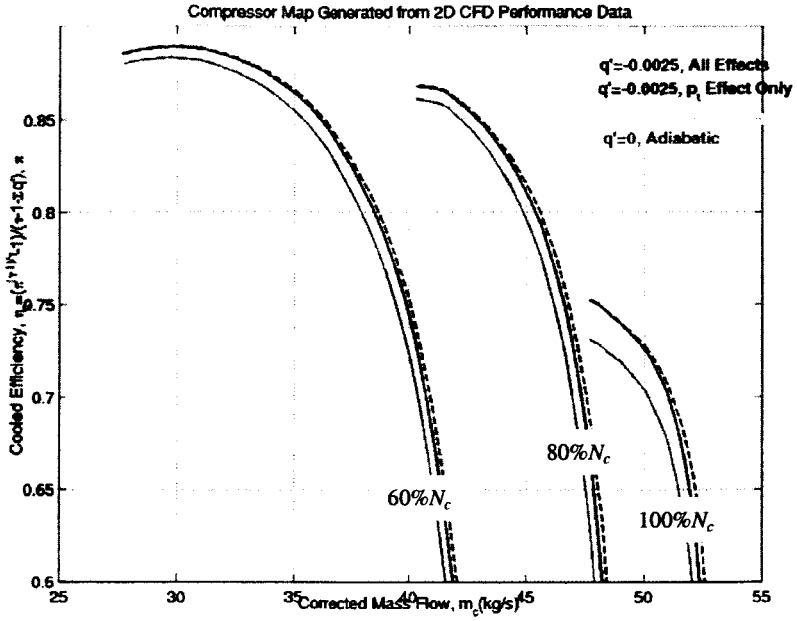

Figure 28: Single stage efficiency map, with and without different effects from cooled cascade performance. Solid red line is adiabatic; solid green line shows cooling effects of change in deviation only; dashed black line shows cooling effects of change in ω only; dashed blue line shows both effects. 100%, 80%, and 60% N_c lines are shown. q`=-0.001

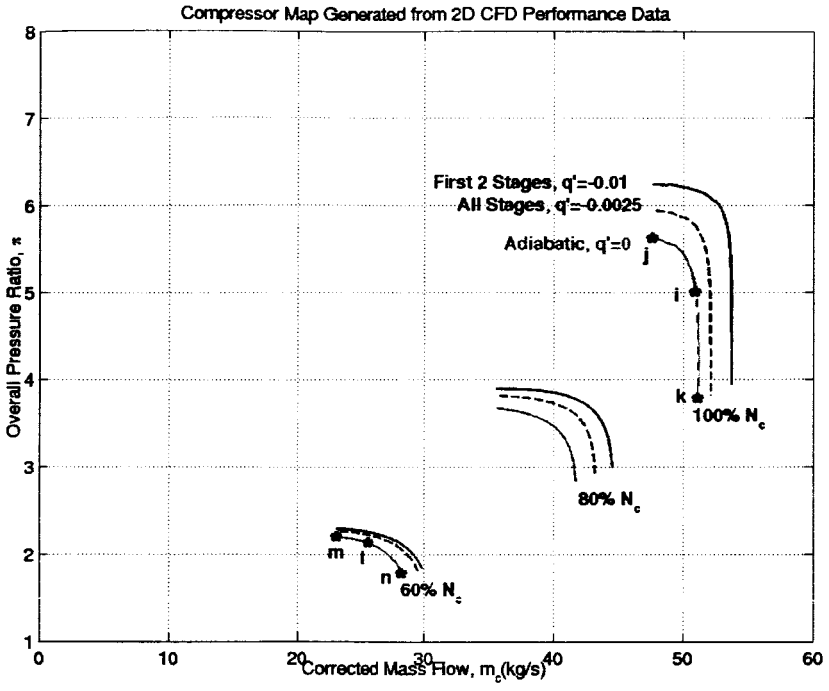

Figure 29a: Eight stage compressor map, with and without cooling. Solid red line is adiabatic; solid green line is q`=-0.01 in the last two stages; dashed blue line is q`=-0.0025 in all stages; solid black line is q`=-0.01 in first two stages. 100%, 80%, and 60% N_c lines are shown.

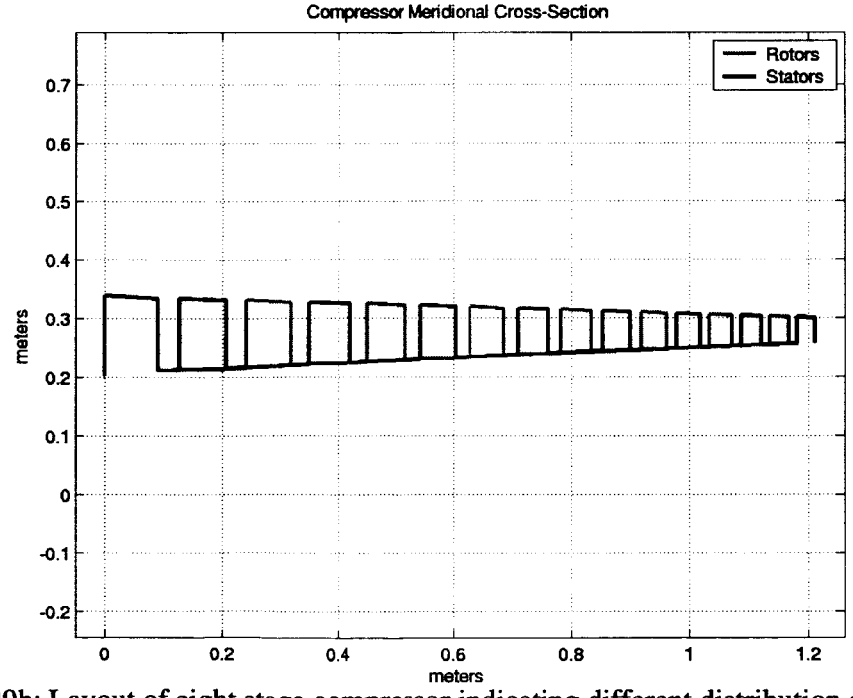

Figure 29b: Layout of eight stage compressor indicating different distribution of cooling

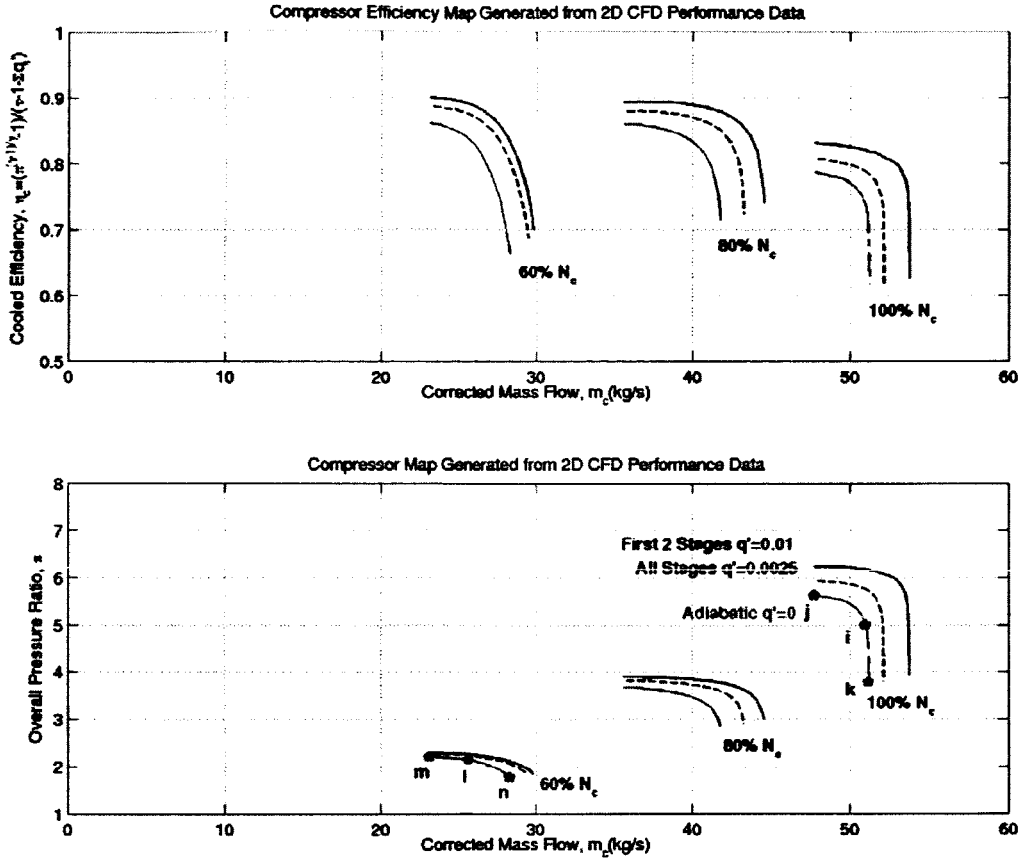

Figure 30: Eight stage compressor map and the corresponding efficiency map with and without cooling.

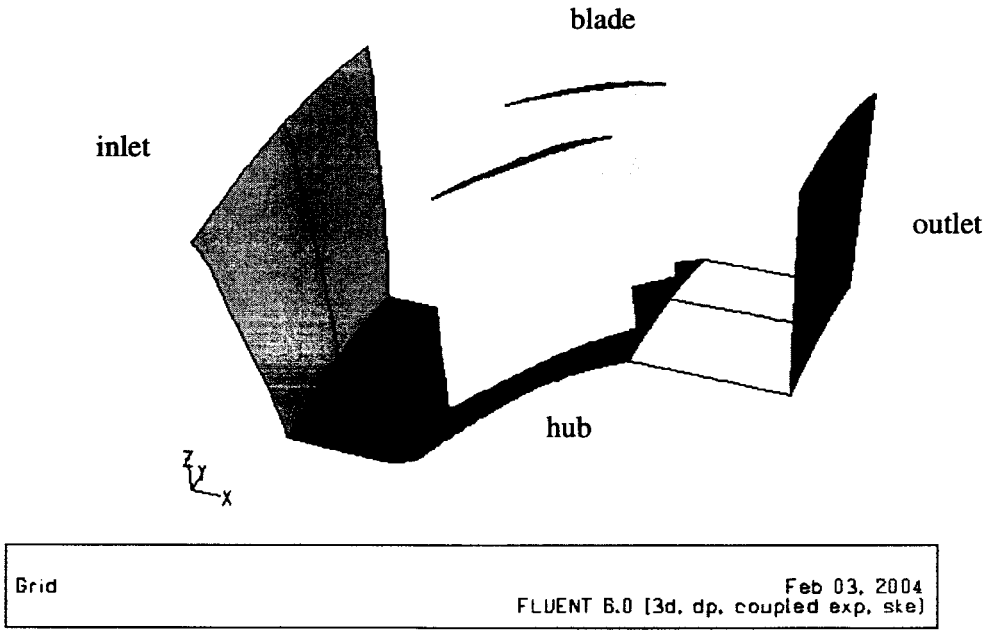

Figure 31a: Computational domain for the NASA High-speed stage 35 rotor

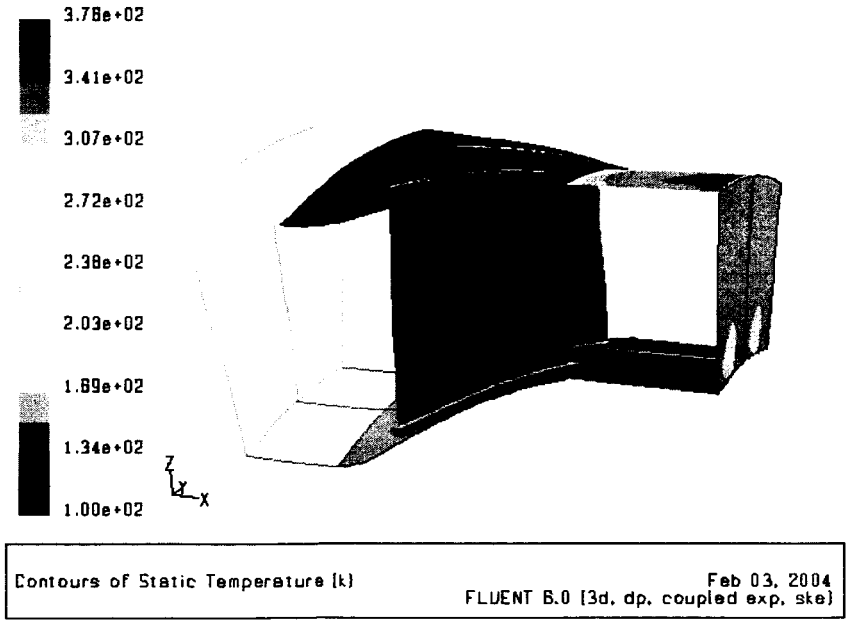

Figure 31b: Temperature distribution of surfaces of flow path in NASA Stage 35 rotor passage.

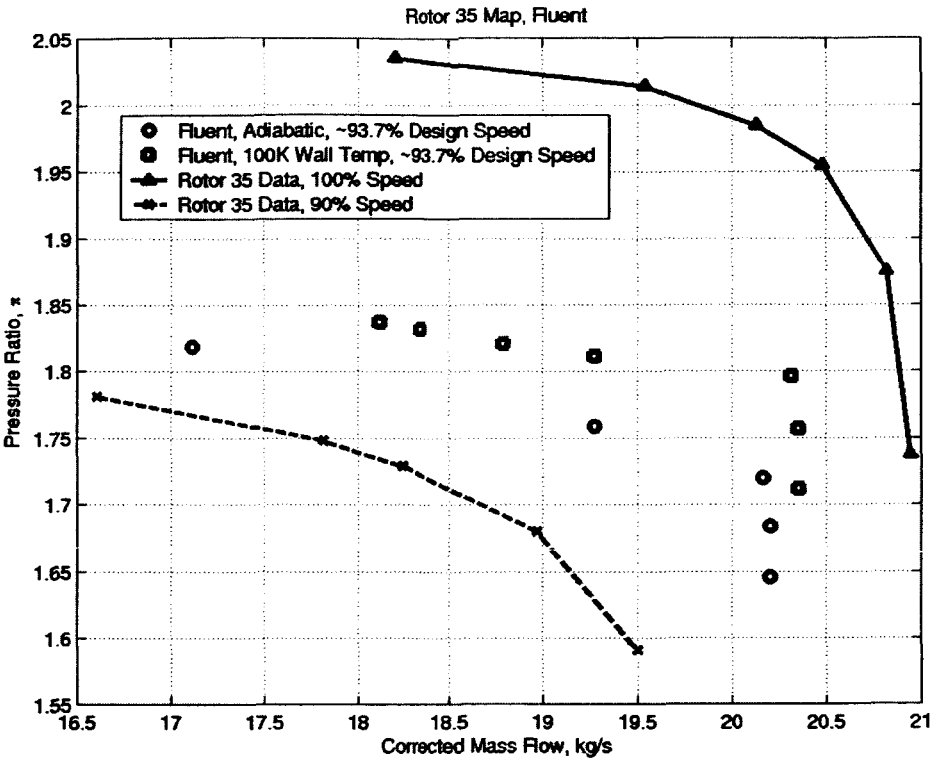

Figure 32: Computed Pressure Rise Characteristic of Adiabatic and Cooled Stage 35 Rotor at 93.7% Corrected Speed for Comparison with Measurements at 90% and 100% Corrected Speed